Journal of Functional Foods 132 (2025) 106963

Contents lists available at ScienceDirect

Journal of Functional Foods

journal homepage: www.elsevier.com/locate/jff

Therapeutic potential of *Gynura procumbens* in enhancing cytokine regulation in the cervix of rats induced by 7,12-dimethylbenz(*a*) anthracene: In vivo and in silico investigations

Putri Cahaya Situmorang [a,*], Syahputra Wibowo [b], Syafruddin Ilyas [a], Sony Eka Nugraha [c], Alexander Patera Nugraha [d], Diyah Tri Utami [e], Nik Mohd Afizan Nik Abd Rahman [f], Rizal Mukra [g]

[a] *Departmentof Biology, Faculty of Mathematics and Natural Sciences, Universitas Sumatera Utara, Medan, Indonesia*
[b] *Eijkman Research Center for Molecular Biology, National Research and Innovation Agency (BRIN), Cibinong, Bogor 16911, Indonesia*
[c] *Department of Pharmaceutical Biology, Faculty of Pharmacy, Universitas Sumatera Utara, Medan, Indonesia*
[d] *Department of Orthodontic, Faculty of Dental Medicine, Universitas Airlangga, Surabaya, Indonesia*
[e] *Department of Pharmacy, School of Vocational, Universitas Sebelas Maret, Surakarta, Indonesia*
[f] *Department of Cell and Molecular Biology, Faculty of Biotechnology and Biomolecular Sciences, Universiti Putra Malaysia. Selangor Darul Ehsan, Malaysia*
[g] *Department of Biology, Faculty of Mathematics and Natural Sciences, State Universitu of Medan, Indonesia*

ARTICLE INFO

Keywords:
Cancer
Gynura procumbens
IL-1β IL-6
IL-10
IL-18

ABSTRACT

Cytokine dysregulation plays a central role in DMBA-induced cervical inflammation with neoplastic potential. This study investigated the effects of *Gynura procumbens* (GB) on key cytokines—IL-1β, IL-6, IL-10, and IL-18—using in vivo and in silico approaches. Female rats treated with DMBA received GB extract at 100, 200, or 300 mg/kg weight. GB at 300 mg/kg significantly suppressed IL-1β and IL-18 ($p < 0.01$) while restoring IL-10 to near-normal levels. IL-6 expression, reduced by DMBA, was upregulated following GB treatment. Histology revealed reduced epithelial damage and improved regeneration. In silico analysis showed that GB's active compounds, particularly nonanedioic and tetradecanoic acids, had higher binding affinity to IL-10 and IL-18 than cisplatin. Molecular dynamics simulations indicated enhanced protein stability, with RMSF values reduced in IL-18 (from 4.7 Å to ~2.7 Å) and IL-10 (from 6.2 Å to ~3.1 Å). These results support the anti-inflammatory and immunomodulatory potential of GB for cervical inflammation with neoplastic features.

1. Introduction

7,12-Dimethylbenz[*a*]anthracene (DMBA) is a polycyclic aromatic hydrocarbon (PAH) primarily employed in research as a potent carcinogen for the study of cancer initiation and progression (Nebert & Dalton, 2006). The role of this molecule in cells is primarily linked to its interactions with DNA and its ability to induce genetic modifications (Conney & Chang, 1991). DMBA is metabolized in cells to form reactive intermediates, such as diol epoxides, through the action of cytochrome P450 enzymes (Baird & Olsson, 1996). These metabolites form covalent bonds with DNA, leading to the creation of DNA adducts that have the potential to induce mutations (Nebert & Dalton, 2006). It often induces mutations in oncogenes or tumor suppressor genes, promoting unregulated cell proliferation. This method is widely employed to induce cancer in animal models, specifically for skin, breast, and liver tumors, to study carcinogenesis (Vannini & Sasso, 2009). The synthesis of reactive oxygen species (ROS) is elevated, leading to cellular damage (Vannini & Sasso, 2009). Increased damage levels can trigger programmed cell death in specific cells. DMBA is essential in developing models for cancer chemoprevention research. The text clarifies the relationship between genetic predispositions and environmental carcinogens (Vannini & Sasso, 2009). DMBA inhibits immune cell function, thereby facilitating tumor evasion from immune surveillance (Vannini & Sasso, 2009). It activates pathways including MAPK and PI3K/AKT,

* Corresponding author at: Study Program of Biology, Faculty of Mathematics and Natural Sciences, Universitas Sumatera Utara, Medan, Indonesia.
E-mail addresses: putri.cahaya@usu.ac.id (P.C. Situmorang), syah031@brin.go.id (S. Wibowo), syafruddin6@usu.ac.id (S. Ilyas), sonyekanugraha@usu.ac.id (S.E. Nugraha), alexander.patera.nugraha@fkg.unair.ac.id (A.P. Nugraha), diyahtriutami12@staff.uns.ac.id (D.T. Utami), m.afizan@upm.edu.my (N.M.A.N.A. Rahman), rizalmukra@unimed.ac.id (R. Mukra).

https://doi.org/10.1016/j.jff.2025.106963
Received 2 December 2024; Received in revised form 9 July 2025; Accepted 14 July 2025
Available online 22 July 2025

which are critical for cellular growth and survival (Li & Zhang, 2015). The role of cytokine regulation is primarily associated with its immunomodulatory and pro-inflammatory characteristics. DMBA exposure can alter immune responses through changes in cytokine expression, often promoting a pro-inflammatory environment (Ma et al., 2018). The synthesis of cytokines, such as tumor necrosis factor-alpha (TNF-α), interleukins (e.g., IL-6), and interferons is stimulated, potentially resulting in chronic inflammation and tumor development (Ma et al., 2018). DMBA concurrently inhibits anti-inflammatory cytokines, including IL-10, thereby exacerbating immunological dysregulation. The effects are mediated by oxidative stress, DNA damage, and the activation of signaling pathways such as NF-κB and MAPK. The imbalance of cytokines creates a tumor-promoting and immunosuppressive environment associated with DMBA exposure (Ma et al., 2018). Research on rats induced with 7,12-dimethylbenz[*a*]anthracene (DMBA) to model cervical carcinogenesis suggests that cytokinins may mitigate oxidative stress and modulate inflammation, which are critical factors in cancer progression (Anisimov et al., 2000). DMBA exposure leads to DNA damage and facilitates carcinogenesis via the production of reactive oxygen species (ROS) and persistent inflammation. Cytokinins are thought to have antioxidant properties that lower ROS levels and may modulate the expression of pro-inflammatory cytokines, thereby inhibiting tumor-promoting pathways (Anisimov et al., 2020). The pro-inflammatory environment facilitates DMBA-induced tumorigenesis by enhancing epithelial cell proliferation and hindering apoptosis (Bostanci & Emingil, 2016). Cytokinin-mediated signaling and DMBA-induced genetic damage work together to initiate and sustain cervical carcinogenesis, highlighting the intricate relationship between hormonal signaling and carcinogenic exposure (Stenbäck et al., 1989). Cytokinins may also affect cell cycle regulation and apoptosis, facilitating the removal of damaged or cancerous cells. The mechanisms indicate a protective or therapeutic potential for cytokinins in DMBA-induced cervical carcinogenesis, necessitating further research to clarify their specific roles and efficacy (Bostanci & Emingil, 2016).

Interleukin-10 and interleukin-6 play a significant role in the progression of cervix-induced DMBA carcinogenesis. IL-10 acts as an anti-inflammatory cytokine, modulating immune responses (Bostanci & Emingil, 2016). The expression in the cervix may affect inflammation, potentially promoting tumor progression by creating a pro-tumorigenic microenvironment. In contrast, IL-6 is a pro-inflammatory cytokine frequently associated with chronic inflammation and cancer progression (Bostanci & Emingil, 2016). In the context of DMBA-induced cervical carcinogenesis, elevated IL-6 levels can promote tumor growth by activating inflammatory pathways, enhancing cell survival, and facilitating angiogenesis Bostanci & Emingil, 2016). The balance between IL-10 and IL-6 influences the immune response, with IL-6 contributing to carcinogenesis and IL-10 potentially inhibiting tumor development. However, IL-10 may prove ineffective in the presence of strong inflammatory signals induced by DMBA (Choi & Lee, 2020). IL-18 plays a role in the development and progression of cervical tumors. DMBA exposure can trigger inflammatory responses, leading to the upregulation and release of IL-18, which subsequently activates immune cells, including T-cells and macrophages. The inflammatory microenvironment causes cellular changes that may promote tumorigenesis in the cervix (Choi & Lee, 2020). IL-18 may enhance the expression of multiple inflammatory mediators, resulting in increased cell proliferation, angiogenesis, and immune evasion, thus promoting the carcinogenic effects of DMBA in the cervix. IL-18 plays a significant role in the inflammatory pathways that facilitate cervical tumorigenesis triggered by DMBA (Gopalakrishnan & Thompson, 2022). Interleukin-1 beta (IL-1β) plays a crucial role in inflammation and immune response, with significant research focused on its involvement in cervical cancer and other diseases. IL-1β plays a role in the initiation and progression of cervical cancer in the context of cervix-induced carcinogenesis (Gopalakrishnan & Thompson, 2022). In models of DMBA-induced cervical carcinogenesis, the administration of IL-1β enhances cervical inflammation, thereby fostering an environment conducive to cancer development (Lee & Lee, 2018). IL-1β induces the release of various pro-inflammatory cytokines and chemokines, which activate signaling pathways that can lead to DNA damage, tumor initiation, and increased cancer progression. In DMBA-induced cervical carcinogenesis, IL-1β promotes tumor growth and metastasis through the establishment of a chronic inflammatory microenvironment (Lee & Lee, 2018). The inflammatory environment facilitates the recruitment of immune cells and the synthesis of growth factors that enhance tumorigenesis. IL-1β regulates key enzymes and proteins involved in cell proliferation, apoptosis, and angiogenesis (Lee & Lee, 2018). This cytokine can accelerate the carcinogenic process in combination with DMBA, known for its ability to induce DNA adducts and mutations (Pereira & Silva, 2020). The overall impact of IL-1β in this model highlights its potential role in promoting cervical cancer through both direct and indirect mechanisms (Pereira & Silva, 2020).

Gynura procumbens (GB) is a native plant species discovered in Indonesia. The term frequently employed by folks in Indonesia is "Sambung Nyawa". The plant's leaves are used to make a decoction, which is employed as a medicinal treatment to improve antioxidant health and protect against many diseases (Tan et al., 2016). Various studies have extensively documented the numerous advantageous properties of the leaves of this plant. These properties include the ability to lower blood pressure, protect the heart, reduce high blood sugar levels, enhance fertility, prevent cancer growth, combat bacterial infections, neutralise harmful free radicals, safeguard organs, reduce inflammation, and inhibit the growth of cancer cells (Hew et al., 2013). *Gynura procumbens'* ethanol extract stops reactive oxygen species (ROS) and pro-inflammatory cytokine mediators from being produced, therefore slowing down the progression of UV-B-induced matrix metalloproteinases 1 (MMP-1) and 9 (Lee et al., 2011). In MDA-MB-231 cells, Proliferation markers Ki67 and PCNA were shown to express less when the SN-F11/12 molecule was present, also known as the invasion marker CCL2 (Giri et al., 2023). This suggests that SN-F11/12 might have a cell-harming mechanism of action. Examining *Gynura procumbens* as a tactic was the driving force for this research (Hew et al., 2013). DMBA was administered to rats to establish an animal model of cervical inflammation. Our study hypothesizes that *Gynura procumbens* may possess anti-inflammatory and immunomodulatory properties, which have the potential to alleviate cytokine dysregulation induced by DMBA, a known carcinogen. Furthermore, integration of in vivo and in silico investigations may elucidate the interactions and molecular processes involved in its therapeutic efficacy.

2. Material and methods

2.1. Reagents

The reagents used for the ELISA approach were the following: ELISA Kit IL-1β PitokineR (EKO393-CAP), ELISA Kit Rat IL-6 (#*E*-E1-R0015) from Elabscience, Rat IL-10 ELISA Kit (#ab214566) and Rat IL-18 ELISA Kit (#ab213909) from Abcam, USA. The antibodies utilised for Immunohistochemistry were Invitrogen IL-1β Polyclonal Antibody (#PA5–119221) Invitrogen IL-6 Monoclonal Antibody (#AHC0762), Invitrogen IL-10 Polyclonal Antibody (#PA5–94918) and Invitrogen IL-18 Polyclonal antibody (#PA5–79481) From ThermoFisher Scientific, USA. Furthermore, a phosphate-buffered saline (PBS) solution was employed, which consisted of a 50 % glycerol and 1 % bovine albumin (BSA) buffer (Catalogue Number BS-0812R).

2.2. Preparation of Gynura procumbens (GB) leaves

GB leaves were gathered in Samosir, a region located in the North Sumatra Province of Indonesia. A solution was prepared by dissolving 5 kilogrammes of GB leaves in 5 l of 70 % ethanol. The solution was then subjected to maceration and evaporation processes, resulting in the production of 150 grammes of concentrated extract. The conversion of

GB into nano chitosan extract involved the utilisation of a chitosan solution prepared by combining chitosan with a glacial acetic acid solution in a 1:1 ratio. The mixture was stirred for 24 h and then filtered using Whatman paper. The Na-TPP solution was prepared by agitating Na-TPP in distilled water for a duration of two hours. The Sambung Nyawa extract will be dissolved in the Na-TPP solution. The Sambung nyawa extract was added to the Na-TPP solution and combined with the chitosan solution using a magnetic stirrer in the process of nano-encapsulation. Additionally, there was a leakage from the hypodermic carrying the catechin solution. The chitosan solution was agitated at a temperature of 280 °C for a duration of 15 min following the complete addition of the Sambung Nyawa solution.

2.3. Animal handling

A total of 36 female *Rattus norvegicus* were utilised for this study. Female rats reach sexual maturity around 11–14 weeks of age and have a weight ranging from 180 to 200 grammes. Each cage housed a total of six female rats. The female rats were acclimated to the laboratory environment for a duration of two weeks. The laboratory environment maintained a steady temperature of 25.3 degrees Celsius and a humidity level ranging between 35 and 60 %. The female rats were housed in an environment with uninterrupted lighting and provided with unrestricted access to water and a meal consisting of maize and pellets throughout the day. The research conducted by USU's FMIPA Medan Medical Research Ethics Committee has been accepted under the reference number 0910/KEPH-FMIPA/2023

2.4. Research design

This study employed an experimental research methodology, utilising a completely randomised design. Female rats were acclimated for a period of two weeks prior to being administered a subcutaneous injection of 7,12-dimethylbenz(*a*)anthracene (DMBA) into the cervix at a dosage of 50 mg per kilogramme of body weight (excluding group C). After a period of three months, the rats developed protuberances in the vicinity of the cervix. Consequently, a biopsy was conducted to ascertain the malignancy of the growth. If the analysis confirms that the lump is a tumor, the rats are categorised into six treatment groups. These groups include group C, which serves as the negative control (representing normal conditions). Additionally, there are two other groups: C-, consisting of rats induced by DMBA, and C+, consisting of rats induced by DMBA and treated with 4 mg/kg BW cisplatin. GB1 are rat that was administered with DMBA + Sambung Nyawa leaves at a dosage of 100 mg/kg BW, while GB2 are rat that received DMBA + Sambung Nyawa leaves at a dosage of 200 mg/kg BW. GB3 are rat that received DMBA + Sambung Nyawa leaves at a dosage of 300 mg/kg BW. The administration of this herbal remedy is done through oral ingestion. The cervix was dissected for immunohistochemistry analysis, while blood samples were collected for ELISA investigation

2.5. Measurement of haematological parameters

Aseptic pipette is employed to extract cardiac blood samples. In order to prevent the rupture of red blood cells, contact with water is abstained from. Furthermore, a microcentrifuge plate was supplemented with 0.5 ml of anticoagulant and 10 ml of EDTA per 1 ml. The Medan City Health Laboratory conducts hematology analyses. As per the manufacturer's specifications, each sample underwent three analyses.

2.6. Enzyme-linked immunosorbent assay (ELISA)

Blood is drawn from the heart into a tube containing an anticoagulant such as EDTA or citrate. After being stored at room temperature for 10–20 min, the vials were centrifuged at a speed of 2000–3000 rpm for 20 min. Subsequently, the collected liquid portion can be analysed. We initiated the procedure by employing a microplate containing 10 wells to generate our standard. In wells 1 and 2, we combined 100 ul of the standard with 50 ul of standard diluent. Subsequently, we moved 100 ul from each of these wells to wells 3 and 4. We replicated this procedure for wells 5 and 6, 7 and 8, and 9 and 10. Subsequently, we introduced antibody capture into each well and subjected the plate to incubation for a duration of 30 min at a temperature of 37 °C or alternatively, overnight at a temperature of 4 °C. We prepared a 30-fold dilution of the wash solution by dissolving 1 ml of the solution in 29 ml of distilled water (Simanullang et al., 2022a). Following the process of draining the wells, we proceeded to cleanse them thoroughly by washing them five times using the wash solution that was created in Step 3. The sample was treated with a blocking reagent to guarantee that the antigen stuck to the plate. Based on the specific requirement, the plate was thereafter incubated in an incubator set at 37 °C for either 24 or 60 min (Situmorang et al., 2024a). Ten microliters of sample and forty microliters of sample diluent were added to each well after the incubation period to get the sample ready. The specimen should be positioned at the bottom of the well. The next thing to do is combine the sample and diluent samples thoroughly. Set the temperature of the incubator to a warm but not too hot setting and let the plates in there for 120 min. Fill up every well with 100 m with biotinylated antibody. After the initial 60 min of incubation, the plate should be left at 37 °C for another full day. The next step is to drain the wells and disinfect them using the washing solution you made in Step 3. Repeat this process five times. Each well should be filled with 100 μl of the ABC solution. For 30 min, keep the temperature at 37 °C (Situmorang et al., 2024b). After that, use the washing solution you made in Step 3 to clean the wells five times until they are empty. Thereafter, 90 ul of HRP conjugate and 90 ul of TMB were added to each well. The dish needs thirty minutes in a preheated oven at 37 °C Every well turned yellow after 100 ul of blocking solution was injected, turning the blue hue back to blue. A 450 nm wavelength measurement using an ELISA reader is required to ascertain the optical density (OD) value (Simanullang et al., 2022b).

2.7. Immunohistochemistry

Cervical tissue is soaked in xylol I and II for a duration of ten minutes. The preparations should be immersed in absolute alcohol I, II, III, 95 % alcohol, 80 % alcohol, and 70 % alcohol consecutively for a duration of 5 min each. This should be followed by two 2-min rinses with deionized water. Immerse the preparations in a solution of citric acid buffer with a concentration of 0.01 M and a pH of 6.0. During the process of boiling, place the tissue in the microwave and heat it for a duration of 10 min, ensuring that it does not get dry. Immerse the jar in liquid and allow it to reach a lower temperature. Once the treatment has cooled down, proceed to rinse it in PBS (pH 7.4) for a duration of three minutes (Manurung et al., 2021: Ilyas et al., 2019). On three occasions. Gradually applying a 3 % solution of hydrogen peroxide (H_2O_2) onto slides inhibits the activity of cell peroxidase. After 15 min in a 30 % H2O2 solution at room temperature, wash the slides thrice for three minutes in PBS. Following the rinsing of the absorbent paper with PBS, a solution containing 5 % normal serum and a secondary antibody from a species that is comparable was added. Subsequently, a block was performed at a temperature of 37 °C for a duration of 30 min (Situmorang & Ilyas, 2018). Prior to injecting the primary antibody dilution, remove any excess moisture from the tissue by using absorbent paper. Input the value only if PBS lacks a negative control. Following incubation with diluted primary antibodies (IL-1β, IL-6, IL-10, and IL-18), the slides were placed in a container with moisture and maintained at a temperature of 4 °C for the duration of the night. Upon optimising the antibody dilution, a discovery was made. Following three 2-min washes with PBS, the slides were dried using absorbent paper and then subjected to re-incubation at a temperature of 37 degrees Celsius for a duration of 30 min with an HRP-conjugated secondary antibody. Following a three-minute washing process repeated four times, drying with absorbent

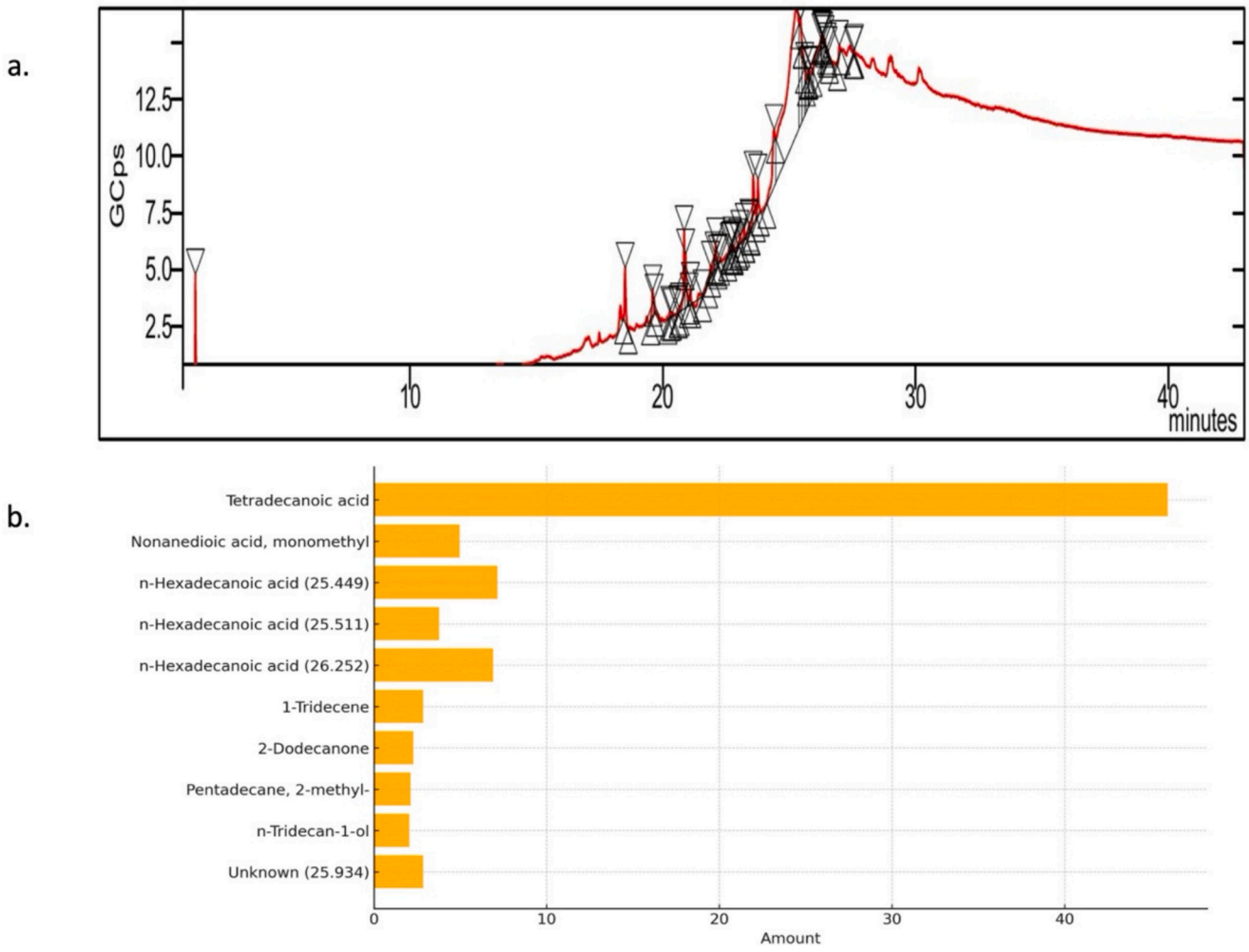

Fig. 1. GC–MS analysis of *Gynura procumbens* ethanol extract. (a) Total Ion Chromatogram (TIC) depicting the distribution of detected compounds over retention time. (b) Bar chart of the top 10 identified compounds based on amount (area %), derived from TIC data.

paper, and subsequent infiltration with DAB substrate, tissue sections can be examined using a microscope. It is recommended to choose shades of brown or golden-brown. Adequate surveillance is necessary to prevent excessive intensification of the colour, however water can halt a reaction. The process of hematoxylin staining involves immersing the specimen in Harris hematoxylin solution for approximately 30 s, rinsing it with water, submerging it in a solution of 1 % alcohol and hydrochloric acid, and then rinsing it again. Immerse the object in a series of solutions containing 70 %, 80 %, 90 %, and 95 % concentration of absolute alcohol I and II, xylol I and II, respectively. After two minutes in each solution, rinse with water. Finally, dry the object in a fume hood. The slide was covered with a microscope and ready to be examined.

2.8. Data Minings

The compounds used in the in silico analysis were sourced from the PubChem database, with the corresponding PubChem IDs listed as follows: DMBA (6001), Cisplatin (5702198), Tetradecanoic acid (11005), n-Hexadecanoic acid (985), and Nonanedioic acid (2266). For proteins, we utilised the Protein Data Bank (PDB) from the UniProt database. The UniProt codes are as follows: P97636 for IL-18, P29456 for IL-10, P20607 for IL-6, and Q63264 for IL-1β. The proteins used in the in silico analysis are derived from *Rattus norvegicus*, making them representative models for the in vivo data.

2.9. Molecular docking

The docking simulation was performed using cavity-detection-guided Blind Docking through CB-Dock2, an enhanced version of the CB-Dock server designed for protein-ligand blind docking. This method combines cavity detection, docking, and homologous template fitting. CB-Dock2 identifies binding sites automatically, determines their center and size, adjusts the docking box size based on the ligands in question, and carries out molecular docking using AutoDock Vina. The process is streamlined with CB-Dock, which enhances accuracy by predicting target protein binding sites through a curvature-based cavity detection method (CurPocket) and determining ligand binding poses with AutoDock Vina.

2.10. Molecular dynamics simulation

Molecular dynamics simulations of IL-18, IL-10, IL-6, and IL-1β, along with Cisplatin as a control and ligands with the best binding affinities, were performed using the CABS-flex 2.0 webserver (http://biocomp.chem.uw.edu.pl/CABSflex2). This system calculates RMSF (root mean square fluctuation) values with strong correlation to NMR data. CABS-flex offers high-resolution (10-ns) near-native protein dynamics simulations, making it effective for real-time evaluation of protein-ligand stability. The simulations were run with default settings, including 50 cycles and 50 trajectory frames of 10 ns each, with additional distance restraints applied (global weight 1.0) [Wibowo et al.,

Table 1
GCMS results of *Gynura procumbens* (GB).

No	RT	Peak Name	Molecular Formula	Area	Amount	R.Match	Concentration (%)
1	1.507	Methyl Alcohol	CH_4O	7.819e+9	1.868	832	1.868
2	18.511	Pentadecane, 2-methyl-	$C_{16}H_{34}$	8.889e+9	2.123	843	2.123
3	19.598	11-Bromoundecanoic acid	$C_{11}H_{21}BrO_2$	3.523e+9	0.841	658	0.841
4	19.653	n-Tridecan-1-ol	$C_{13}H_{28}O$	1.821e+9	0.435	819	0.435
5	20.273	cis-9-Tetradecen-1-ol	$C_{14}H_{28}O$	8.933e+8	0.213	786	0.213
6	20.360	9-Tetradecen-1-ol, (E) -	$C_{14}H_{28}O$	3.199e+8	0.076	810	0.076
7	20.589	Undecanoic acid, hydroxy-, lactone	$C_{11}H_{20}O_2$	2.365e+8	0.056	778	0.056
8	20.654	11-Hexadecen-1-ol, (Z) -	$C_{16}H_{32}O$	3.525e+8	0.084	827	0.084
9	20.843	1-Tridecene	$C_{13}H_{26}$	1.197e+10	2.858	826	2.858
10	20.902	n-Tridecan-1-ol	$C_{13}H_{28}O$	8.603e+9	2.055	840	2.055
11	21.039	n-Tridecan-1-ol	$C_{13}H_{28}O$	8.517e+8	0.203	818	0.203
12	21.090	Decane	$C_{10}H_{22}$	2.376e+9	0.567	818	0.567
13	21.881	11-Hexadecen-1-ol, (Z) -	$C_{16}H_{32}O$	1.836e+9	0.439	847	0.439
14	22.030	n-Tridecan-1-ol	$C_{13}H_{28}O$	2.946e+9	0.704	799	0.704
15	22.088	n-Tridecan-1-ol	$C_{13}H_{28}O$	3.993e+9	0.954	820	0.954
16	22.156	Undecanoic acid, hydroxy-, lactone	$C_{11}H_{20}O_2$	4.280e+8	0.102	751	0.102
17	22.269	n-Hexadecanoic acid	$C_{16}H_{32}O_2$	2.042e+8	0.049	599	0.049
18	22.624	11-Hexadecen-1-ol, (Z) -	$C_{16}H_{32}O$	6.528e+8	0.156	861	0.156
19	22.683	11-Hexadecen-1-ol, (Z) -	$C_{16}H_{32}O$	7.654e+8	0.183	838	0.183
20	22.730	11-Hexadecen-1-ol, (Z) -	$C_{16}H_{32}O$	1.008e+9	0.241	825	0.241
21	22.757	11-Hexadecen-1-ol, (Z) -	$C_{16}H_{32}O$	3.562e+8	0.085	775	0.085
22	22.807	11-Hexadecen-1-ol, (Z) -	$C_{16}H_{32}O$	2.597e+8	0.062	813	0.062
23	23.046	cis-9-Tetradecen-1-o1	$C_{14}H_{28}O$	9.373e+8	0.224	808	0.224
24	23.222	n-Tridecan-1-ol	$C_{13}H_{28}O$	1.398e+9	0.334	798	0.334
25	23.412	1-Tridecene	$C_{13}H_{26}$	1.189e+9	0.284	755	0.284
26	23.437	1-Tridecene	$C_{13}H_{26}$	6.161e+8	0.147	755	0.147
27	23.576	2-Dodecanone	$C_{12}H_{24}O$	9.548e+9	2.280	923	2.280
28	23.762	Hexadecanoic acid, methyl ester	$C_{17}H_{34}O_2$	5.688e+9	1.359	903	1.359
29	24.400	Nonanedioic acid, monomethyl ester	$C_{10}H_{18}O_4$	2.081e+10	4.971	656	4.971
30	25.273	Tetradecanoic acid	$C_{14}H_{28}O_2$	1.925e+11	45.965	743	45.965
31	25.449	n-Hexadecanoic acid	$C_{16}H_{32}O_2$	2.993e+10	7.149	732	7.149
32	25.511	n-Hexadecanoic acid	$C_{16}H_{32}O_2$	1.580e+10	3.773	725	3.773
33	25.615	n-Hexadecanoic acid	$C_{16}H_{32}O_2$	7.548e+9	1.803	732	1.803
34	25.743	Undecanoic acid, hydroxy-, lactone	$C_{11}H_{20}O_2$	7.134e+9	1.704	572	1.704
35	25.774	Ricinoleic acid	$C_{18}H_{34}O_3$	2.464e+9	0.589	616	0.589
36	25.934	No Match		1.192e+10	2.846		2.846
37	26.252	n-Hexadecanoic acid	$C_{16}H_{32}O_2$	2.888e+10	6.898	673	6.898
38	26.279	Octadecanoic acid	$C_{18}H_{36}O_2$	2.980e+9	0.712	666	0.712
39	26.311	Octadecanoic acid	$C_{18}H_{36}O_2$	5.853e+9	1.398	663	1.398
40	26.366	Pentadecanoic acid	$C_{15}H_{30}O_2$	4.326e+9	1.033	676	1.033
41	26.417	Pentadecanoic acid	$C_{15}H_{30}O_2$	4.391e+9	1.049	670	1.049
42	26.497	n-Hexadecanoic acid	$C_{16}H_{32}O_2$	1.878e+9	0.449	668	0.449
43	26.535	n-Hexadecanoic acid	$C_{16}H_{32}O_2$	8.436e+8	0.201	679	0.201
44	26.981	9-Octadecenoic acid (*Z*)-, methyl ester	$C_{19}H_{36}O_2$	1.818e+9	0.434	645	0.434
45	27.577	Hexadecanoic acid, 2,3-dihydroxypropyl ester	$C_{19}H_{38}O_4$	1.822e+8	0.044	611	0.044

2024; Wibowo et al., 2021; Wibowo et al., 2022].

2.11. Statistical analysis of data

The In vivo data are presented with the mean and standard deviation before analysis using ANOVA followed by Duncan's follow-up test. The Kruskall-Wallis test was employed to study non-parametric data, and a Mann-Whitney test was portrayed as a follow-up. Developing hypotheses, presenting data, computing test statistics, and coming to a conclusion are all aspects of the testing process.

3. Results

3.1. Gas chromatography-mass spectroscopy profiling of Gynura procumbens

The presence of over 20 distinct chemicals with varying phytochemical activity was detected using GC–MS analysis of *Gynura procumbens*. Fig. 1 depicts the chromatogram acquired during analysis, provided that a more comprehensive chromatogram analysis may be found in the supplemental file. The retention time (RT), molecular formula, molecule weight, and detected R.match of Chemical composition in *Gynura procumbens* are presented in Table 1, Fig. 1–2 and Supplementary file figure.

Fig. 1 depicts the GC–MS profile of the ethanol extract of Gynura procumbens, elucidating its phytochemical makeup. Panel (a) presents the Total Ion Chromatogram (TIC), showcasing multiple sharp and distinct peaks within a retention time span of about 1 to 40 min. The existence of several peaks signifies a complex and varied amalgamation of volatile and semi-volatile phytoconstituents. Panel (b) displays a bar chart illustrating the ten most prevalent compounds identified from the chromatogram. Tetradecanoic acid (RT 25.27 min) was identified as the predominant compound, succeeded by nonanedioic acid, monomethyl ester, and other derivatives of n-hexadecanoic acid, which were observed at several retention times. The fatty acids and their derivatives possess anti-inflammatory, antioxidant, and cytoprotective activities, potentially enhancing the therapeutic efficacy of *G. procumbens*. The integrated chromatographic and quantitative analysis robustly substantiates the premise that GB encompasses a range of bioactive lipophilic substances, perhaps contributing to its therapeutic effectiveness. The outcomes of all substances are presented in Table 1 and Fig. 2. These findings also provide a basis for subsequent isolation and bioactivity-guided fractionation investigations.

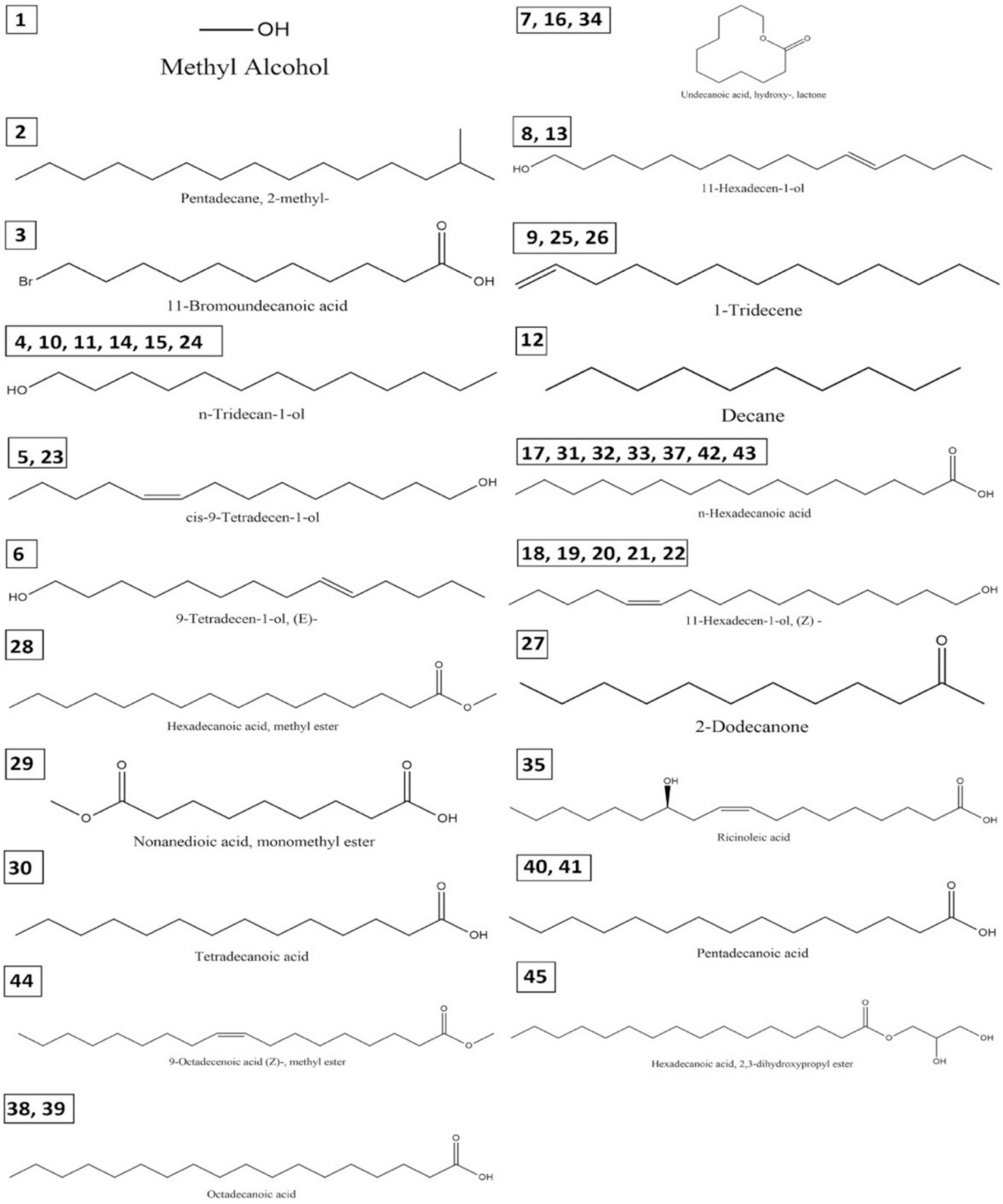

Fig. 2. The composition results of *Gynura procumbens* (GB) reveal its chemical structure.

3.2. Effect of Gynura procumbens on haematological markers in rats with cancer

The haematological parameters in the cancer mouse model were altered following the administration of cisplatin (in the comparison group) and *Gynura procumbens* (Sambung Nyawa) leaves at a dosage of 100–300 mg/kg BW, as indicated in Table 2. The haematological measures exhibited considerable disparities among the control groups (C), C- (cancerous rats without therapy), and after the injection of Cisplatin (C+). The SGOT and SGPT levels exhibited a notable disparity between the *Gynura procumbens* 200 mg/kg BW (GB2) group and the C- group. Significant differences ($p < 0.01$) were observed in the concentrations of haemoglobin, leukocytes, lymphocytes, eosinophils, monocytes, SGOT, SGPT, and creatinine between the experimental group and the control group when GB3 was administered at a dose of 300 mg/kg body weight (C-). The control comparison group, however, showed comparable values (C+). Neither the neutrophil count nor the hematocrit nor the urea levels varied significantly between the categories ($p > 0.05$). The haematological data presented in Table 3 indicates that the administration of *Gynura procumbens* at doses of 100–300 mg/kg BW had an

Table 2
Effect of *Gynura procumbens* on Hematology parameters of cancer rats.

Parameters	Unit	Groups (Mean ± SD)					
		C	C-	C+	GB1	GB2	GB3
Erythrocytes	x10^6/μL	8.20 ± 0.21	10.01 ± 0.01$^{\#}$	8.59 ± 0.02	10.24 ± 1.04	9.91 ± 0.14	8.80 ± 0.02
Leukocytes	x 10^3/μL	9.09 ± 0.13	14.18 ± 0.91$^{\#}$	9.22 ± 0.13*	13.26 ± 1.05	13.22 ± 1.32	10.11 ± 0.07 *
Haemoglobin	g/dL	12.91 ± 0.21	28.95 ± 2.03$^{\#\#}$	17.42 ± 2.01*	28.98 ± 2.81	24.12 ± 1.98	20.14 ± 2.31*
Monocytes	x 10^3/μL	0.392 ± 0.01	0.981 ± 0.01 $^{\#}$	0.413 ± 0.01*	0.942 ± 0.021	0.903 ± 0.01	0.400 ± 0.01 *
Lymphocytes	x 10^3/μL	5.16 ± 0.02	8.95 ± 0.04$^{\#}$	6.91 ± 0.04*	8.97 ± 1.04	8.12 ± 0.13	5.92 ± 0.03*
Eosinophils	x 10^3/μL	0.049 ± 0.01	0.067 ± 0.0	0.060 ± 0.0	0.062 ± 0.01	0.065 ± 0.01	0.055 ± 0.01
Neutrophils	x 10^3/μL	0.052 ± 0.01	0.098 ± 0.01 $^{\#}$	0.044 ± 0.01*	0.097 ± 0.01	0.096 ± 0.01	0.045 ± 0.01
Creatinine	mg/dL	0.46 ± 0.01	0.77 ± 0.01$^{\#}$	0.44 ± 0.01*	0.69 ± 0.02	0.68 ± 0.02	0.50 ± 0.01*
Ureum	mg/dL	22.23 ± 1.11	37.03 ± 2.32$^{\#}$	23.21 ± 3.15*	37.41 ± 2.14	36.12 ± 1.23	30.11 ± 1.25
SGOT	u/L	124.88 ± 7.22	245.12 ± 5.31$^{\#\#}$	200.07 ± 6.21*	239.15 ± 9.18	200.86 ± 9.81*	198.02 ± 6.21* *
SGPT	u/L	59.26 ± 4.15	169.37 ± 5.01$^{\#\#}$	100.29 ± 9.01*	160.21 ± 8.92	155.21 ± 8.37*	134.29 ± 4.21*
Hematocrit	%	42.13 ± 2.24	45.28 ± 2.72	45.20 ± 3.21	45.03 ± 2.01	44.01 ± 3.27	42.10 2.33

Note: C: Untreated, C-: rats induced by DMBA, C+: rats induced by DMBA +4 mg/kg BW cisplatin, GB1: rats induced by DMBA +100 mg/Kg BW of GB, GB2: rats induced by DMBA +200 mg/Kg BW of GB, GB3: rats induced by DMBA +300 mg/Kg BW of GB, The results are expressed as mean ± standard deviation ($n = 6$, $^{\#}p < 0.05$ vs C, $^{\#\#}p < 0.01$ vs C, *p < 0.05 compared C-, **p < 0.01 vs C-).

Table 3
The IL-1β expression in cervical tissue after administration of *Gynura procumbens.*

Groups	The comparison between two groups (p value)					
	C	C-	C+	GB1	GB2	GB3
C		0.0010	0.040	0.040	0.040	0.040
C-			0.001	0.001	0.001	0.001
C+				0.060	0.040	0.040
GB1					0.040	0.040
GB2						0.040
GB3						

Note: C C: Untreated, C-: rats induced by DMBA, C+: rats induced by DMBA +4 mg/kg BW cisplatin, GB1: rats induced by DMBA +100 mg/Kg BW of GB, GB2: rats induced by DMBA +200 mg/Kg BW of GB, GB3: rats induced by DMBA +300 mg/Kg BW of GB,.

impact on the haematological parameters of rats. However, the levels of erythrocytes, eosinophils, hematocrit, and urea were found to be within the normal range. Administration of *Gynura procumbens* at a dose of 100–300 mg/kg BW affected the haematological parameters of rats, as indicated by the haematological results. Nevertheless, the levels of erythrocytes, eosinophils, hematocrit, and urea were determined to be within the acceptable range. It is possible to achieve normal test results in certain cases, despite the presence of cancer.

3.3. IL-1β expression in cervical histological alterations and serum following the administration of Gynura procumbens

Analysed rats blood serum to ascertain the expression of IL-1β, after administering *Gynura procumbens* leaves. The minimum dosage exhibited the greatest IL-1β expression and did not display any significant variation in the C- group. *Gynura procumbens*, also known as Sambung Nyawa, effectively suppressed the expression of IL-1 β at a dosage of 300 mg/kgBW, as shown in Fig. 3. The Kruskal-Wallis test conducted on nonparametric data revealed a noteworthy disparity in IL-1β expression across the different groups, as indicated in Table 5. A statistically significant difference in IL-1β expression was found between the C-group and the other groups in the Mann-Whitney test (p < 0.01). The control group did not show a statistically significant change ($p < 0.05$) when GB was administered at a dosage of 200 mg/kg body weight (GB2) (C-). The results of the testing in the blood serum and table are supported by the histological changes in cervical tissue caused by the expression of IL-1β. The group C- endometrial epithelial structure exhibits a significant abundance of columnar epithelium. While certain cells possess cilia, the majority are equipped with surface microvilli. This epithelial structure is associated with its role as a place where the embryo can be implanted. GB3 administration results in the transformation of the endometrial epithelium into a singular cuboidal epithelium, with the absence of visible cilia. This phenomenon arises from the shedding of the outermost layer of the mucous membrane, resulting in the erosion of the cylindrical epithelium at the surface. Consequently, only the basal epithelial cells, which have a cuboidal form, remain intact (Fig. 4, Table 3).

3.4. IL-6 expression in cervical histological alterations and serum following the administration of Gynura procumbens

The analysis results indicated that the comparison group (C+) exhibited the greatest levels of IL-6, followed by the normal group (C) and the highest dose (GB3). Cancer can lead to a reduction in the expression of IL-6 (C-). Even at the minimum dosage, *Gynura procumbens* effectively inhibits the synthesis of GB1 groups. The expression of IL-6 was increased at doses of 200 and 300 mg/kgBW, however the average value differed from the comparison group (Fig. 5). The expression levels of IL-6 showed significant differences between groups ($p < 0.01$) according to the study of cancer histology using the Mann-Whitney test ($p < 0.00$, $p = 0.001$, Table 4, Fig. 6). From a histological perspective, the tissue exhibits a weakening of the epithelium, referred to as cervical atrophy, as a result of its resemblance to squamous epithelial cells. *Gynura procumbens* leaves stimulate the proliferation of epithelial maturation, particularly in cervical cells, hence promoting the formation and production of new cervical cells. The administration of *Gynura procumbens* leaves resulted in the observed reduction of squamous epithelial cells in malignancy. In cancer, the production of IL-1β is reduced when the dosage of Gynura procumbens is increased (100-300 mg/kgBW). *Gynura procumbens* exhibits a significant amount of polyphenols, particularly kaempferol, which can enhance the synthesis of IL-6. The production of IL-6 is impaired in cervical cancer.

3.5. IL-10 expression in cervical histological alterations and serum following the administration of Gynura procumbens

The blood serum of cervical cancer model rats was also examined for IL-10 expression. Research showed that increasing the dosage to 100 mg/kg BW (GB1) had no discernible effect on IL-10 expression. Fig. 7 demonstrates a substantial elevation in IL-10 expression at dosages of 300 and 300 mg/kgBW (GB2 and GB3). Nevertheless, the histological Mann-Whitney test revealed that GB3 exhibited the highest level of expression, which was nearly identical to that of the untreated group (C). dosage At a dosage of 100 mg/kg BW of *Gynura procumbens,* When comparing the cervical histopathology analysis to the control groups (C- and C+), there was no statistically significant difference seen. Nevertheless, there was a notable disparity in the blood serum concentrations

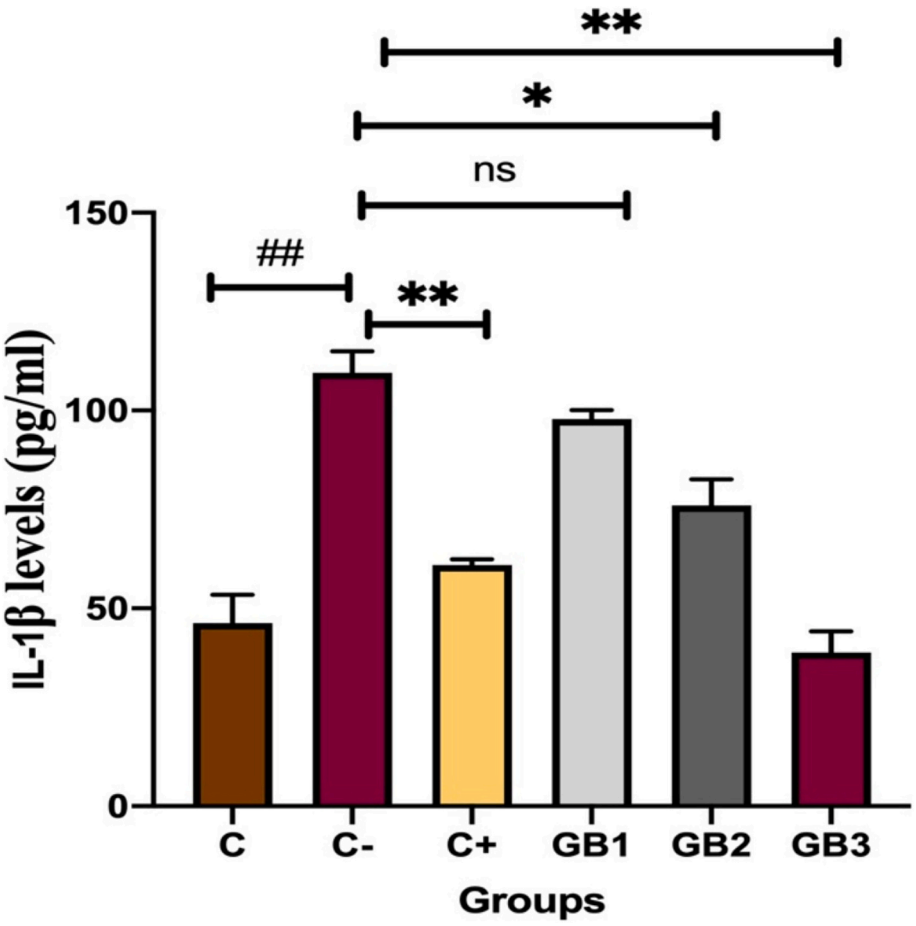

Fig. 3. Levels of IL-1β in cervical rats. C: Untreated, C-: rats induced by DMBA, C+: rats induced by DMBA +4 mg/kg BW cisplatin, GB1: rats induced by DMBA +100 mg/Kg BW of GB, GB2: rats induced by DMBA +200 mg/Kg BW of GB, GB3: rats induced by DMBA +300 mg/Kg BW of GB, The results are expressed as mean ± standard deviation ($n = 6$, $^{\#}p < 0.05$ vs C, $^{\#\#}p < 0.01$ vs C, *p < 0.05 compared C-, **p < 0.01 vs C-).

as assessed using ELISA analysis. Histologically, it is evident that group C suppresses cellular mitosis and growth, affecting not just normal cells but also those undergoing hyperplasia and exhibiting hypertrophic characteristics, such as cancer cells. Subsequently, the tissue undergoes heightened proliferation of epithelial maturation, resulting in the thickening of vaginal cells. This process also affects cervical cells, particularly those in the outer part of the cervix (ectocervix), leading to an increase in epithelial maturation proliferation. However, the administration of *Gynura procumbens* starts to diminish the maturation of cells in the cervix, which is most pronounced at the highest dosage (Fig. 8). Histological and protein studies revealed that the administration of the highest dosage resulted in an upregulation of IL-10 expression in rats with a cervical cancer model (Table 5).

3.6. IL-18 expression in cervical histological alterations and serum following the administration of Gynura procumbens

A serum analysis was performed to evaluate the expression of IL-18 in cervical rats. The findings demonstrated a decline in IL-18 expression at every dosage level, with the lowest expression observed in the untreated group (C), followed by the groups treated with cisplatin at doses of 300 and 200 mg/kgBW (Fig. 9). Statistically significant differences in IL-18 expression were found between the groups in the histological analysis that used the Kruskal-Wallis test. We found no statistically significant change in the expression of this protein between the C and GB3 groups when we applied the Mann-Whitney test. However, in comparison to the C- group, they exhibited distinct variations in IL-18 expression ($p < 0.01$, $p = 0.001$). Additionally, histology reveals the existence of adipose tissue. Excessive fat accumulation within cells leads to increased workload for cell organelles, particularly the Golgi apparatus, as they strive to convert this fat into compounds that can disrupt cellular functioning. Groups GB1 and GB2 exhibited a clear and spacious lumen, with the epithelium being consistently organised. Group C exhibited a very slender lumen, with a relatively thin endometrial region and loosely organised constituent cells. Additional epithelial cells are present in the lumen, originating from the mucosal region of the epithelium, resulting in a reduction in thickness of the epithelium. The epithelial cells have undergone lysis, resulting in apparent tissue vascularization. The adherence of the epithelium to the glands causes thinning of the lamina propria (Table 6, Fig. 10). The administration of GB leaf extract induces alterations in the cellular composition of the cervix. Histologically, alterations were observed at doses of 200 and 300 mg/kg BW. In these cases, the GB1 group, which received the lowest dose, had the highest expression of IL-18, similar to the group of rats with the cervical model. The administration of *Gynura procumbens* leaf extract induces improvements in the proliferating cervical cellular tissue. Microscopically, alterations were detected at doses of 200 and 300 mg/kg body weight. The GB1 group, which was administered the lowest dose, exhibited the highest expression of IL-18, akin to the group of rats with a model of cervical cancer.

3.7. Molecular docking and molecular dynamic simulation of IL-18

Molecular docking of DMBA with IL-18 showed a binding energy of −7.0 kcal/mol, involving Pi-alkyl interactions with LYS A:60, a Pi-donor hydrogen bond with SER A:108, and van der Waals forces with ARG

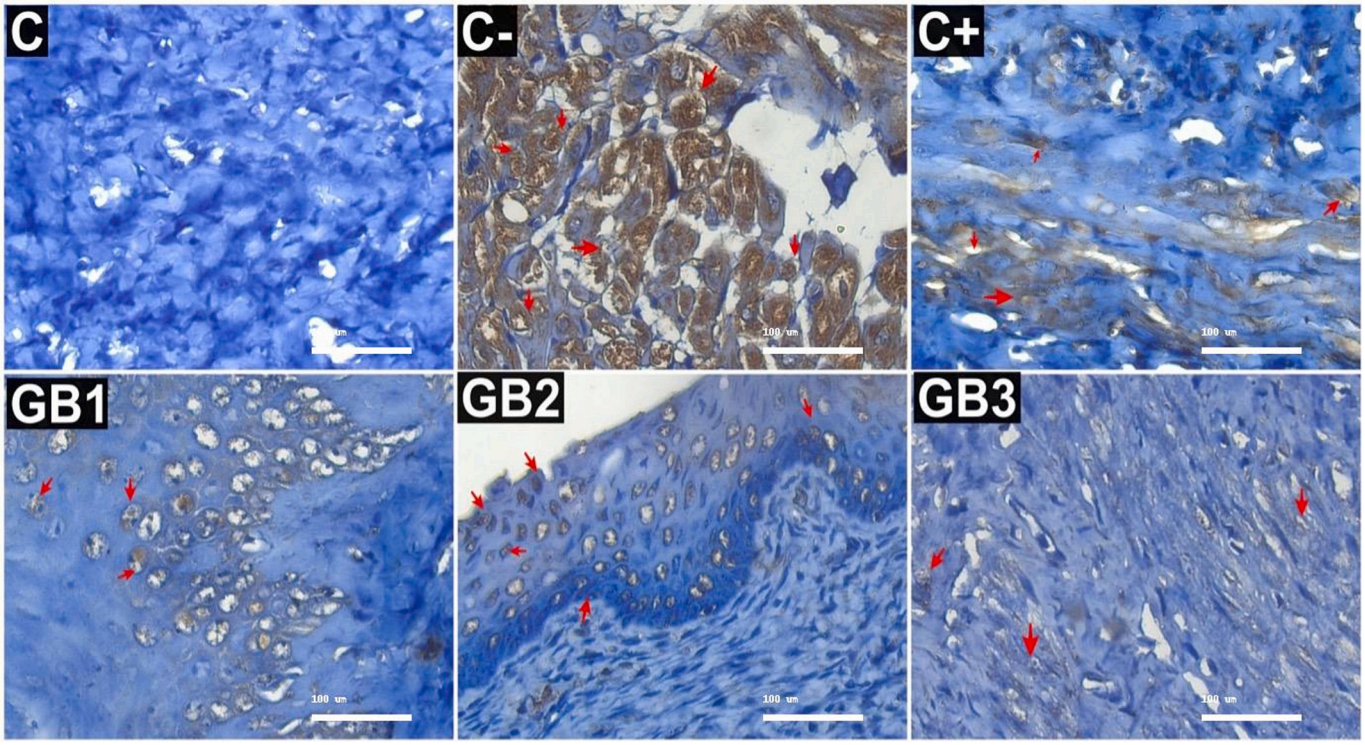

Fig. 4. Expression of IL-1β in histology of cervical rats. C: Untreated, C-: rats induced by DMBA, C+: rats induced by DMBA +4 mg/kg BW cisplatin, GB1: rats induced by DMBA +100 mg/Kg BW of GB, GB2: rats induced by DMBA +200 mg/Kg BW of GB, GB3: rats induced by DMBA +300 mg/Kg BW of GB. Red arrows indicate areas of positive IL-1β expression. Scale bar represents 100 μm (400×). (For interpretation of the references to colour in this figure legend, the reader is referred to the web version of this article.)

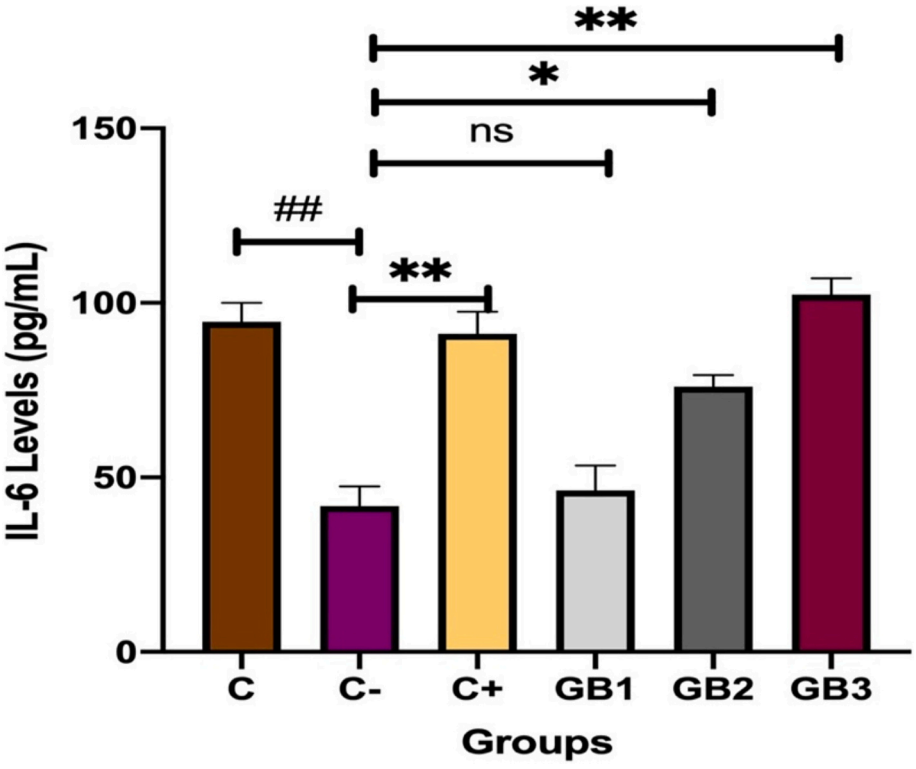

Fig. 5. Levels of IL-6 in cervical rats. C: Untreated, C-: rats induced by DMBA, C+: rats induced by DMBA +4 mg/kg BW cisplatin, GB1: rats induced by DMBA +100 mg/Kg BW of GB, GB2: rats induced by DMBA +200 mg/Kg BW of GB, GB3: rats induced by DMBA +300 mg/Kg BW of GB, The results are expressed as mean ± standard deviation ($n = 6$, $^{\#}p < 0.05$ vs C, $^{\#\#}p < 0.01$ vs C, *p < 0.05 compared C-, **p < 0.01 vs C-).

Table 4
The IL-6 expression in cervical tissue after administration of *Gynura procumbens*.

Groups	The comparison between two groups (p value)					
	C	**C-**	**C+**	**GB1**	**GB2**	**GB3**
C		0.0010	0.036	0.036	0.036	0.100
C-			0.036	0.036	0.036	0.0010
C+				0.100	0.100	0.0010
GB1					0.100	0.036
GB2						0.036
GB3						

Note: C Untreated, C-: rats induced by DMBA, C+: rats induced by DMBA +4 mg/kg BW cisplatin, GB1: rats induced by DMBA +100 mg/Kg BW of GB, GB2: rats induced by DMBA +200 mg/Kg BW of GB, GB3: rats induced by DMBA +300 mg/Kg BW of GB.

A:106/61, VAL A:58/102, ASP A:59/104, PHE A:119, and ASN A:62 (Fig. 11). In contrast, cisplatin exhibited weaker binding (−1.0 kcal/mol), forming a hydrogen bond with ASP A:130 and van der Waals interactions with PHE A:38, HIS A:37, ASP A:36/90, SER A:91, and ILE A:131. Nonanedioic acid bound the IL-18–DMBA complex with −5.1 kcal/mol, forming hydrogen bonds with GLU A:15/34 and van der Waals interactions with LEU A:25/33, GLU A:28, LYS A:14/89, ILE A:26, PRO A:27, PHE A:13, ASN A:12, and MET A:16. Similarly, n-hexadecanoic acid showed −4.6 kcal/mol binding energy, with hydrogen bonds to GLU A:15 and ILE A:26, Pi-alkyl interactions with PHE A:13, alkyl contacts with LEU A:25/33, MET A:16, LYS A:14, and van der Waals interactions with ASN A:12, SER A:91, LYS A:89, and GLU A:28/34.

In the context of IL-18, DMBA, as the negative control, leads to significant flexibility, with RMSF values peaking at 4.7 Å (residue 15) and 4.2 Å (residue 90). These high values reflect a lack of stabilization, as expected from a negative control, where the protein structure remains quite dynamic. Cisplatin, the positive control, offers a moderate level of stabilization, with peaks at 4.5 Å (residue 18) and 4.4 Å (residue 95). While cisplatin reduces flexibility compared to DMBA, some regions of the protein still exhibit noticeable movement. Nonanedioic acid, the active compound in this context, shows clear improvement over both controls. Residue 85 has an RMSF of 3.1 Å, and residue 130 measures at 2.9 Å in Fig. 12. These lower values indicate that nonanedioic acid stabilizes IL-18 more effectively than cisplatin, keeping the protein structure more rigid and reducing dynamic fluctuations. This suggests that nonanedioic acid might offer superior stabilization of IL-18 compared to the commercial drug cisplatin. As previously mentioned, nonanedioic acid demonstrated improved stabilization of IL-18 compared to the controls. Delving deeper into the data, residues between 70 and 100 consistently show lower RMSF values across the nonanedioic acid complex, particularly residues 75 and 92, which display values of around 2.7 Å and 3.0 Å, respectively. This pattern of stability is absent in both DMBA and cisplatin complexes. For DMBA, these same regions exhibit values as high as 4.0 Å, suggesting that nonanedioic acid uniquely stabilizes these mid-regions of IL-18. Residue 70 in the DMBA complex shows an RMSF of 3.9 Å, whereas nonanedioic acid significantly lowers the flexibility to just 2.8 Å. Further supporting these findings, the overall distribution of RMSF values across IL-18 shows that nonanedioic acid provides more consistent stabilization across the entire protein. While DMBA displays a sharp peak around residues 15–30, the nonanedioic acid complex smooths out this fluctuation, especially from residue 20, where RMSF drops to 2.5 Å compared to the higher 4.7 Å seen with DMBA. The suppression of these large fluctuations indicates that nonanedioic acid may engage in more effective interactions with IL-18, potentially leading to better therapeutic applications by stabilizing essential regions of the protein structure.

3.8. Molecular docking and molecular dynamic simulation of IL-10

Molecular docking of IL-10 with DMBA showed a binding energy of −7.0 kcal/mol, involving Pi-sigma interaction with LEU A:91, Pi-alkyl

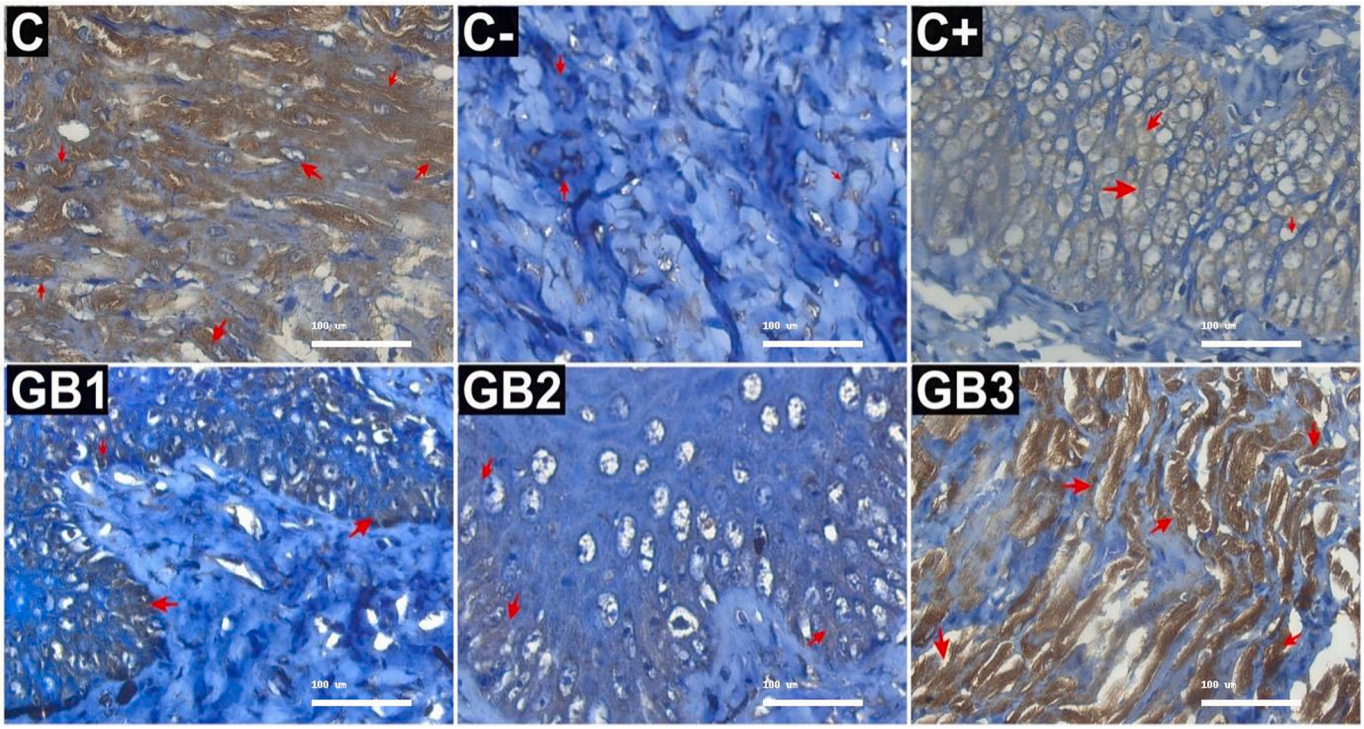

Fig. 6. Expression of IL-6 in histology of cervical rats. C: Untreated, C-: rats induced by DMBA, C+: rats induced by DMBA +4 mg/kg BW cisplatin, GB1: rats induced by DMBA +100 mg/Kg BW of GB, GB2: rats induced by DMBA +200 mg/Kg BW of GB, GB3: rats induced by DMBA +300 mg/Kg BW of GB. Red arrows indicate areas of positive IL-6 expression. Scale bar represents 100 μm (400×). (For interpretation of the references to colour in this figure legend, the reader is referred to the web version of this article.)

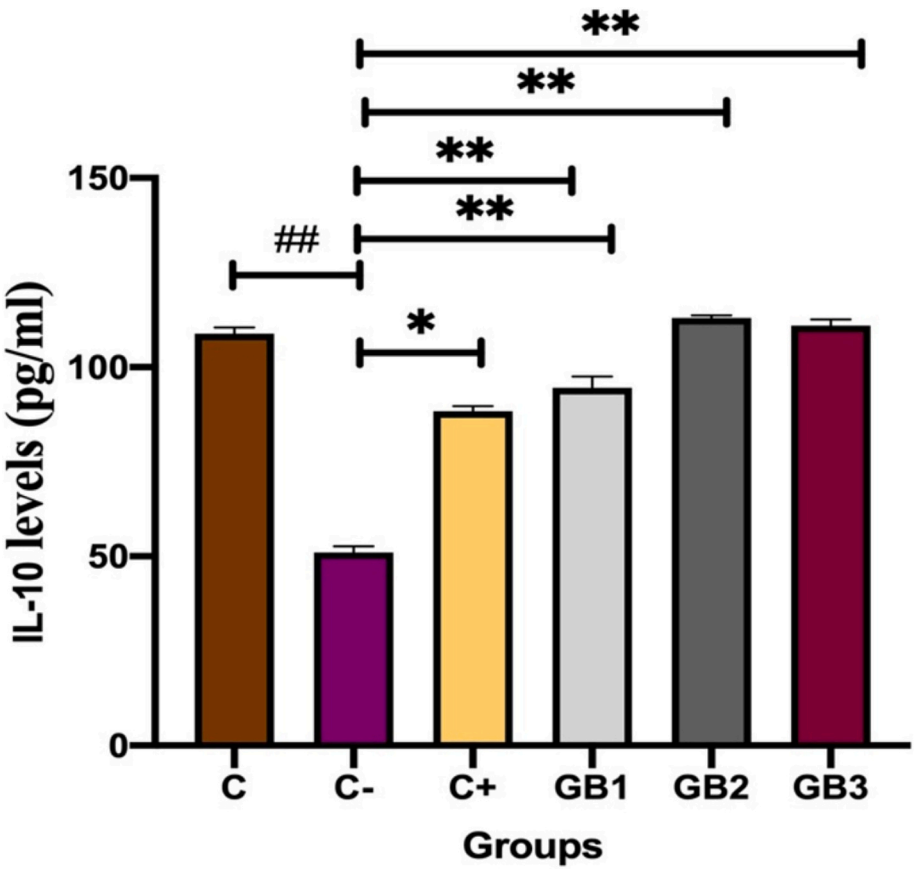

Fig. 7. Levels of IL-10 in cervical rats C: Untreated, C-: rats induced by DMBA, C+: rats induced by DMBA +4 mg/kg BW cisplatin, GB1: rats induced by DMBA +100 mg/Kg BW of GB, GB2: rats induced by DMBA +200 mg/Kg BW of GB, GB3: rats induced by DMBA +300 mg/Kg BW of GB, The results are expressed as mean ± standard deviation ($n = 6$, $^{\#}p < 0.05$ vs C, $^{\#\#}p < 0.01$ vs C, *p < 0.05 compared C-, **$p < 0.01$ vs C-).

interactions with VAL A:92, LYS A:117, and PRO A:96, and van der Waals contacts with TRP A:120, GLU A:99/114, and GLY A:113. In contrast, cisplatin exhibited a weaker binding energy (−1.1 kcal/mol), forming hydrogen bonds with LEU A:65 and ILE A:64, and van der Waals interactions with VAL A:142, THR A:67, ASN A:63, and ASP A:145. n-Hexadecanoic acid bound at −3.9 kcal/mol, forming hydrogen bonds with THR A:31, ASN A:28, and CYS A:30, along with Pi-alkyl interactions with PHE A:129 and PRO A:34, and van der Waals/alkyl contacts with MET A:176 and ARG A:128 (Fig. 13). Nonanedioic acid showed −4.3 kcal/mol binding energy, with hydrogen bonds to GLN A:122, ARG A:125, and ASP A:27, plus van der Waals interactions with ASN A:28/29, CYS A:30/126, and PHE A:33. Tetradecanoic acid bound at −4.2 kcal/mol via hydrogen bonding with SER A:84, Pi-alkyl contacts with TRP A:120 and ARG A:124/125, and alkyl/van der Waals interactions with ILE A:121, LEU A:130, and CYS A:132. These docking results support the in vivo data, where nonanedioic and tetradecanoic acids—administered at 200–300 mg/kg BW, effectively restored IL-10 levels, reinforcing their potential in modulating inflammatory responses. With IL-10, DMBA, the negative control, induces high flexibility, with RMSF values reaching 6.2 Å (residue 20) and 4.5 Å (residue 65). This is in line with DMBA's role as a negative control, showing poor stabilization of the protein. Cisplatin, as the positive control, also shows significant flexibility in IL-10, with RMSF peaking at 7.4 Å (residue 18) and 6.0 Å (residue 68). This high level of movement indicates that while cisplatin binds to IL-10, it does not greatly stabilize the protein, allowing for substantial fluctuations. Nonanedioic acid, on the other hand, demonstrates better performance than cisplatin. The RMSF peaks at 3.8 Å (residue 25) and 3.2 Å (residue 70) indicate much lower flexibility. These reduced values suggest that nonanedioic acid binds more effectively to IL-10, stabilizing the structure and restricting dynamic movement. Compared to the positive control, nonanedioic acid shows significant improvement in stabilizing IL-10.

In the IL-10 + nonanedioic acid complex, residues 20–30 display striking reductions in RMSF values when compared to the DMBA and cisplatin complexes (Fig. 14). Residue 22, for instance, exhibits an RMSF of 3.1 Å with nonanedioic acid, significantly lower than the 6.0 Å seen with DMBA and the 7.0 Å with cisplatin. This marked reduction in flexibility suggests that nonanedioic acid strengthens interactions in the N-terminal region, a critical area that may contribute to the overall structural stability of IL-10. Residue 28 also shows a reduced RMSF of 3.3 Å with nonanedioic acid compared to cisplatin's higher value of 6.8 Å, further confirming its stabilizing role. Interestingly, the central regions of IL-10, particularly residues 50–70, show consistent reductions in RMSF when bound to nonanedioic acid. Residue 65, a key structural component of the protein, shows an RMSF of 3.5 Å with nonanedioic acid, compared to 4.5 Å with DMBA and 6.0 Å with cisplatin. This data implies that nonanedioic acid provides better stabilization across key functional areas of the protein, which could translate to enhanced performance in drug formulations. The stabilization of these regions might help maintain IL-10's functional integrity under physiological conditions.

3.9. Molecular docking and molecular dynamic simulation of IL-6

Molecular docking of IL-6 with DMBA revealed a binding energy of −8.5 kcal/mol, with Pi-anion interactions at GLU A:92/199, Pi-alkyl contacts with LYS A:195 and ALA A:196, Pi-donor hydrogen bonding with ILE A:93, and amide-Pi stacking with VAL A:203. Additional van der Waals interactions were observed with PHE A:200, ASP A:80, LEU A:83/192, and PRO A:91. In contrast, cisplatin showed a much weaker

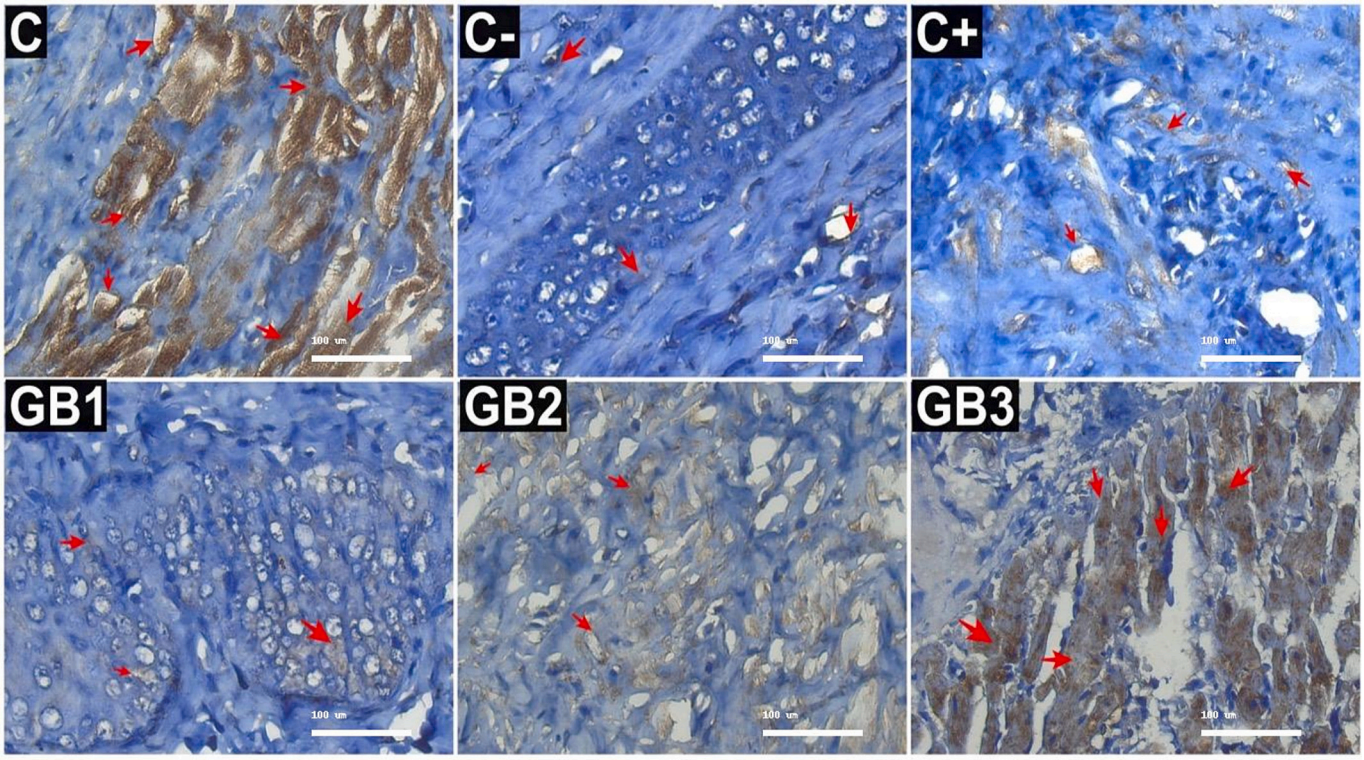

Fig. 8. Expression of IL-10 in histology of cervical rats. C: Untreated, C-: rats induced by DMBA, C+: rats induced by DMBA +4 mg/kg BW cisplatin, GB1: rats induced by DMBA +100 mg/Kg BW of GB, GB2: rats induced by DMBA +200 mg/Kg BW of GB, GB3: rats induced by DMBA +300 mg/Kg BW of GB. Red arrows indicate areas of positive IL-10 expression. Scale bar represents 100 μm (400×). (400×). (For interpretation of the references to colour in this figure legend, the reader is referred to the web version of this article.)

Table 5
The IL-10 expression in cervical tissue after administration of *Gynura procumbens*.

Groups	The comparison between two groups (p value)					
	C	**C-**	**C+**	**GB1**	**GB2**	**GB3**
C		0.0010	0.048	0.048	0.048	0.100
C-			0.048	0.048	0.048	0.0010
C+				0.048	0.048	0.048
GB1					0.100	0.048
GB2						0.048
GB3						

Note: C: Untreated, C-: rats induced by DMBA, C+: rats induced by DMBA +4 mg/kg BW cisplatin, GB1: rats induced by DMBA +100 mg/Kg BW of GB, GB2: rats induced by DMBA +200 mg/Kg BW of GB, GB3: rats induced by DMBA +300 mg/Kg BW of GB.

affinity (−1.1 kcal/mol), forming hydrogen bonds with THR A:48/208 and van der Waals interactions with SER A:49, VAL A:51, GLY A:52, and ARG A:209. n-Hexadecanoic acid bound with −4.2 kcal/mol, displaying a Pi-sigma interaction with TYR A:123, but also an unfavorable donor-donor contact with THR A:167. Additional interactions included Pi-alkyl/alkyl contacts with LEU A:165/174, VAL A:164, PRO A:166, and van der Waals forces with ASN A:171, SER A:170, LYS A:89, and GLU A:119. Nonanedioic acid showed −4.6 kcal/mol binding energy, forming hydrogen bonds with TYR A:123, GLU A:119, LYS A:177, and ASN A:87, along with alkyl and van der Waals contacts involving LEU A:174, LYS A:89, SER A:170, ASN A:86, and PRO A:91/166. Tetradecanoic acid, with a binding energy of −4.7 kcal/mol, engaged in alkyl interactions with LEU A:174 and LYS A:89, and van der Waals interactions with TYR A:123, GLU A:119, PHE A:122, and ASN A:87/171 (Fig. 15). The interaction analysis shows that the active compounds have a stronger binding affinity compared to cisplatin. However, it is important to note that these active compounds work together due to the nature of the crude extract. This means that multiple interactions can occur simultaneously, contributing to the overall effect. Inconsistencies in IL-6 levels, particularly in the GB3 group (rats induced by DMBA +300 mg/kg BW of *Sambung Nyawa*), may be attributed to the presence of n-Hexadecanoic acid and its unfavorable interactions, such as the donor-donor interaction with Threonine (THR A:167). Despite this, the general trend still indicates that the active compounds perform better than cisplatin, reinforcing *Sambung Nyawa's* therapeutic potential.

For IL-6, DMBA, as the negative control, causes high flexibility, with RMSF values reaching 6.4 Å (residue 42) and 5.2 Å (residue 120). This highlights the dynamic behavior of IL-6 in the presence of DMBA, as expected from a negative control. Cisplatin, the positive control, offers moderate stabilization, with peaks at 5.4 Å (residue 40) and 4.3 Å (residue 124). While it reduces flexibility compared to DMBA, IL-6 still exhibits considerable movement in some regions. Tetradecanoic acid, the active compound, performs better than cisplatin. RMSF peaks at 5.0 Å (residue 48) and 3.7 Å (residue 115) suggest that tetradecanoic acid stabilizes IL-6 more effectively, reducing flexibility in key regions. This improvement over cisplatin indicates that tetradecanoic acid could be a stronger stabilizer for IL-6 (Fig. 16). A deeper analysis of IL-6 shows that tetradecanoic acid stabilizes key regions in the protein much more effectively than both the negative control (DMBA) and the positive control (cisplatin). For instance, residues 40–60 show substantial reductions in RMSF values when bound to tetradecanoic acid. Residue 48 has an RMSF of 3.6 Å with tetradecanoic acid, compared to 6.2 Å with DMBA and 5.0 Å with cisplatin. This suggests that tetradecanoic acid significantly dampens the flexibility of this important structural region, enhancing protein stability. Additionally, in the central region of IL-6, residues 100–130 are highly stabilized by tetradecanoic acid. Residue 115, for example, shows an RMSF of just 3.7 Å, while the same residue

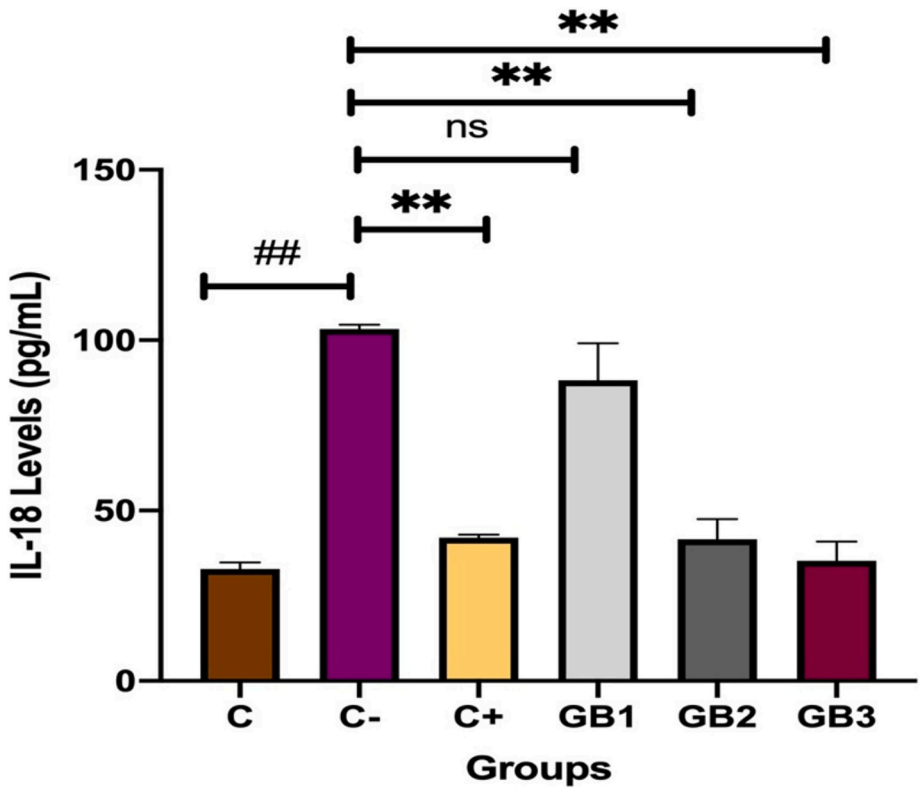

Fig. 9. Levels of IL-18 in cervical rats. C: Untreated, C-: rats induced by DMBA, C+: rats induced by DMBA +4 mg/kg BW cisplatin, GB1: rats induced by DMBA +100 mg/Kg BW of GB, GB2: rats induced by DMBA +200 mg/Kg BW of GB, GB3: rats induced by DMBA +300 mg/Kg BW of GB, The results are expressed as mean ± standard deviation ($n = 6$, $p < 0.05$ vs C, $^{\#\#}p < 0.01$ vs C, *p < 0.05 compared C-, **p < 0.01 vs C-).

Table 6
The IL-18 expression in cervical tissue after administration of *Gynura procumbens*.

Groups	The comparison between two groups (p value)					
	C	**C-**	**C+**	**GB1**	**GB2**	**GB3**
C		0.0010	0.030	0.030	0.030	0.060
C-			0.030	0.100	0.030	0.030
C+				0.100	0.030	0.030
GB1					0.060	0.030
GB2						0.030
GB3						

Note: C: Untreated, C-: rats induced by DMBA, C+: rats induced by DMBA +4 mg/kg BW cisplatin, GB1: rats induced by DMBA +100 mg/Kg BW of GB, GB2: rats induced by DMBA +200 mg/Kg BW of GB, GB3: rats induced by DMBA +300 mg/Kg BW of GB.

fluctuates at 5.0 Å with DMBA and 4.5 Å with cisplatin. This consistent reduction in flexibility across different regions of IL-6 points to tetradecanoic acid as a stronger stabilizer, possibly reducing conformational changes that may affect protein function in therapeutic settings. This pattern of decreased flexibility could make tetradecanoic acid a promising candidate for enhancing the efficacy and stability of IL-6-targeted treatments.

3.10. Molecular docking and molecular dynamic simulation of IL-1β

Molecular docking of IL-1β with DMBA showed a strong binding energy of −8.0 kcal/mol, featuring Pi–Pi stacked and T-shaped interactions with PHE A:92/93, a Pi–sigma interaction with ILE A:96, and van der Waals interactions with PHE A:84/97, PRO A:89, and VAL A:68. In contrast, cisplatin exhibited weaker binding (−1.0 kcal/mol), forming hydrogen bonds with VAL A:163 and PRO A:173, along with van der Waals contacts with PHE A:162 and ILE A:172. n-Hexadecanoic acid bound at −4.8 kcal/mol, forming a hydrogen bond with GLU A:166, Pi–alkyl/Pi–sigma interactions with TRP A:107, alkyl contacts with LYS A:213, and van der Waals interactions with VAL A:216, MET A:211, and ASP A:205. Nonanedioic acid showed a binding energy of −4.7 kcal/mol, with hydrogen bonds to ASP A:110, LEU A:112/113, and Pi–alkyl interaction with TRP A:107. However, an unfavorable acceptor–acceptor interaction with ASP A:109 was also observed. Additional van der Waals contacts occurred with CYS A:104/115 and LYS A:209/210 (Fig. 17). Tetradecanoic acid also bound at −4.7 kcal/mol, forming a hydrogen bond with VAL A:68, alkyl interaction with LEU A:66, and van der Waals interactions with PHE A:93 and ILE A:67. Similar to IL-6, inconsistencies were also observed in the GB1 (rats induced by DMBA +100 mg/kg BW of *Sambung Nyawa*) and GB2 (rats induced by DMBA +200 mg/kg BW of *Sambung Nyawa*) groups, where IL-1β levels were lower than in the cisplatin-treated group. This may be due to the unfavorable acceptor-acceptor interaction involving Nonanedioic acid, which could account for this discrepancy. However, despite this, the overall findings still indicate that the active compounds perform better than cisplatin, underscoring their therapeutic potential.

In the IL-1β + DMBA complex, the negative control shows high flexibility, with RMSF values of 8.2 Å (residue 23) and 6.1 Å (residue 145). These elevated values reflect the protein's dynamic nature when bound to DMBA.Cisplatin, the positive control, shows a significant reduction in flexibility, with RMSF peaks at 6.9 Å (residue 20) and 4.3 Å (residue 140). This indicates that cisplatin stabilizes IL-1β better than DMBA, but some regions still exhibit movement. N-hexadecanoic acid, the active compound, does not perform as well as cisplatin. The RMSF values are higher, with peaks at 9.3 Å (residue 25) and 7.0 Å (residue 135), indicating that n-hexadecanoic acid induces more flexibility in IL-1β compared to the positive control (Fig. 18). This suggests that n-hexadecanoic acid may not offer better stabilization for IL-1β than

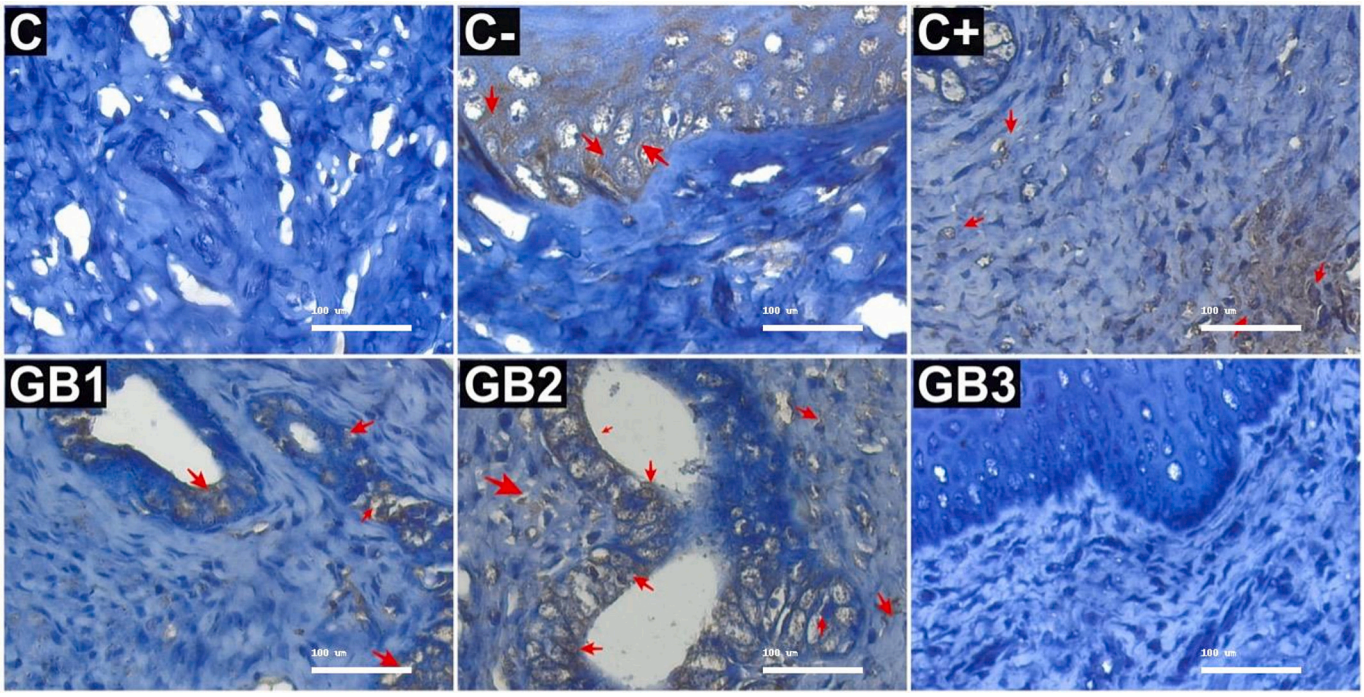

Fig. 10. Expression of IL-18 in histology of cervical rats. C: Untreated, C-: rats induced by DMBA, C+: rats induced by DMBA +4 mg/kg BW cisplatin, GB1: rats induced by DMBA +100 mg/Kg BW of GB, GB2: rats induced by DMBA +200 mg/Kg BW of GB, GB3: rats induced by DMBA +300 mg/Kg BW of GB. Red arrows indicate areas of positive IL-18 expression. Scale bar represents 100 μm (400×). (For interpretation of the references to colour in this figure legend, the reader is referred to the web version of this article.)

cisplatin. In IL-1β, n-hexadecanoic acid introduces significant flexibility, but it is important to note that the RMSF peaks occur predominantly in the N-terminal region, specifically around residues 15–35. Residue 25, for instance, shows an RMSF of 9.3 Å, indicating high flexibility. In contrast, cisplatin demonstrates a more controlled profile, with RMSF values dropping to 6.9 Å in the same region. While n-hexadecanoic acid induces higher flexibility, its effects are localized in this N-terminal region, while the C-terminal and middle residues are not as affected. Further analysis reveals that residues 100–130, which include essential structural components, experience less flexibility in the cisplatin complex compared to n-hexadecanoic acid. Residue 120, for example, shows an RMSF of 4.2 Å with cisplatin but a higher value of 5.9 Å with n-hexadecanoic acid. This suggests that while n-hexadecanoic acid leads to greater flexibility overall, its effects are more pronounced in the N-terminal region, leaving other regions of the protein moderately stabilized. The data reflects that n-hexadecanoic acid might still have potential if the flexibility it induces can be fine-tuned, especially when considering targeted applications in specific protein regions.

4. Discussion

The GCMS study revealed that *Gynura procumbens* (Sambung Nyawa) had elevated concentrations of p-Coumaric acid, p-Hydroxybenzoic acid, and sinapic acid. p-Coumaric acid and p-Hydroxybenzoic acid are polyphenols with the ability to mitigate detrimental conditions associated with inflammation. Sinapic acid suppresses the growth, movement, and infiltration of pancreatic cancer cells by reducing the activity of the AKT/Gsk-3β signaling pathway (Situmorang and ilyas, 2018b). Plant phenolics serve as significant secondary metabolites with the potential to act as anticancer agents (Pande and Rizvi, 2009). Phenolics demonstrate encouraging prospects as cytotoxic anticancer agents due to their ability to inhibit the spread of cancer cells, stimulate programmed cell death, reduce cell division, target the formation of new blood vessels, and regulate cell growth and specialization (Abotaleb et al., 2020). Furthermore, the existence of flavonoids such as Myricetin, Kaempferol, Quercetin, Apigenin, and Rutin was identified. Myricetin plays a role in suppressing cancer growth by controlling the expression of crucial enzymes involved in cancer formation and rapid increase (Rahmani et al., 2023). In regards to cancer-related activities such cell cycle regulation, oxidative stress management, apoptosis induction, cell proliferation control, metastasis inhibition, and angiogenesis suppression, kaempferol demonstrates outstanding antioxidant and anticancer potential (Oattan et al., 2022; Imran et al., 2019). Apigenin possesses the capacity to facilitate cell cycle arrest and stimulate apoptosis through p53-related pathways in human cancer (Shankar et al., 2017). To initiate cell death in cancer cell lines through caspase 8, quercetin compounds activate cell death domains, which in turn activate FAS and FADD (Hashemzaei, 2017). Rutin chemicals target cancer cells by influencing cell cycle arrest, inflammation, oxidative stress, apoptosis, and angiogenesis. They also increase apoptosis and decrease malignant cell development. These effects are all achieved by regulating cancer cellular signaling pathways (Pandey et al., 2021). It is evident that multiple chemicals identified in HPLC analysis exhibit anticancer properties (Pandey et al., 2021).

Administration of *GB* at a dose of 100–300 mg/kg BW affected the haematological parameters of rats, as indicated by the haematological results. Nevertheless, the levels of erythrocytes, eosinophils, hematocrit, and urea were determined to be within the acceptable range. It is possible to achieve normal test results in certain cases, despite the presence of cancer. There is a potential for the test results to fall outside the usual range, even if you are in good condition. There are several reasons why laboratory testing alone are insufficient to definitively diagnose cancer or other disorders (Li et al., 2023). The reduction in WBC count seen after administering this herbal remedy indicates that *Gynura procumbens* includes compounds that can promote the generation of leukocytes and serve as an immune booster. Nevertheless, the levels of many blood parameters are still within the normal range (Li et al., 2023). The impact of cancer on white blood cell counts can vary, with the specific form of cancer, the particular white blood cells involved, and the cancer's location all playing a role (Li et al., 2023; Virdee et al., 2020). Reduced red blood cell count, haemoglobin levels, or hematocrit

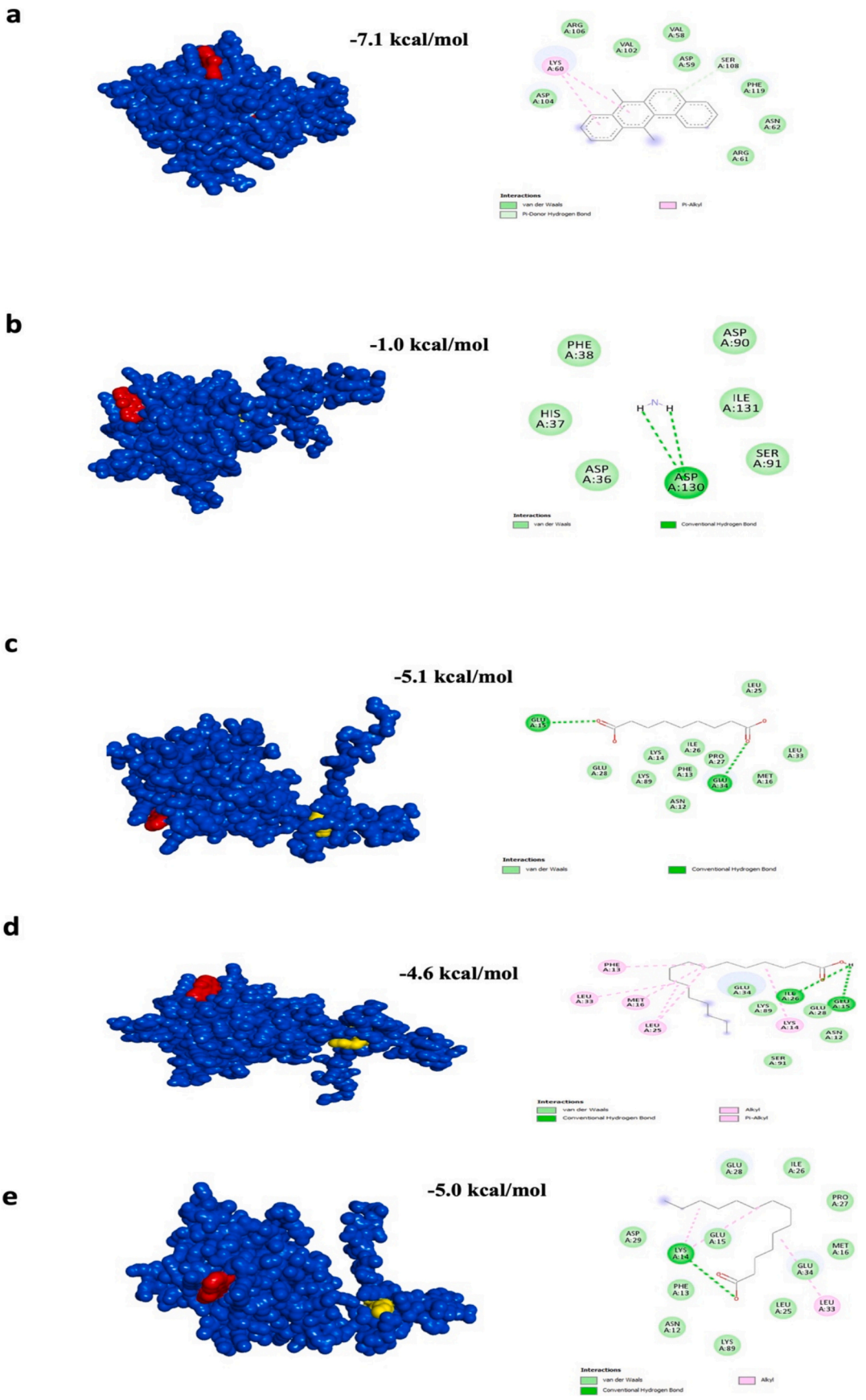

Fig. 11. IL-18 + DMBA (A), (IL-18 + DMBA) + Cisplatin (B), (IL-18 + DMBA) + Nonanedioic acid (C), (IL-18 + DMBA) + n-Hexadecanoic acid (D), (IL-18 + DMBA) + Tetradecanoic acid (E). Each panel shows the molecular surface interaction (left) and 2D binding profile (right).

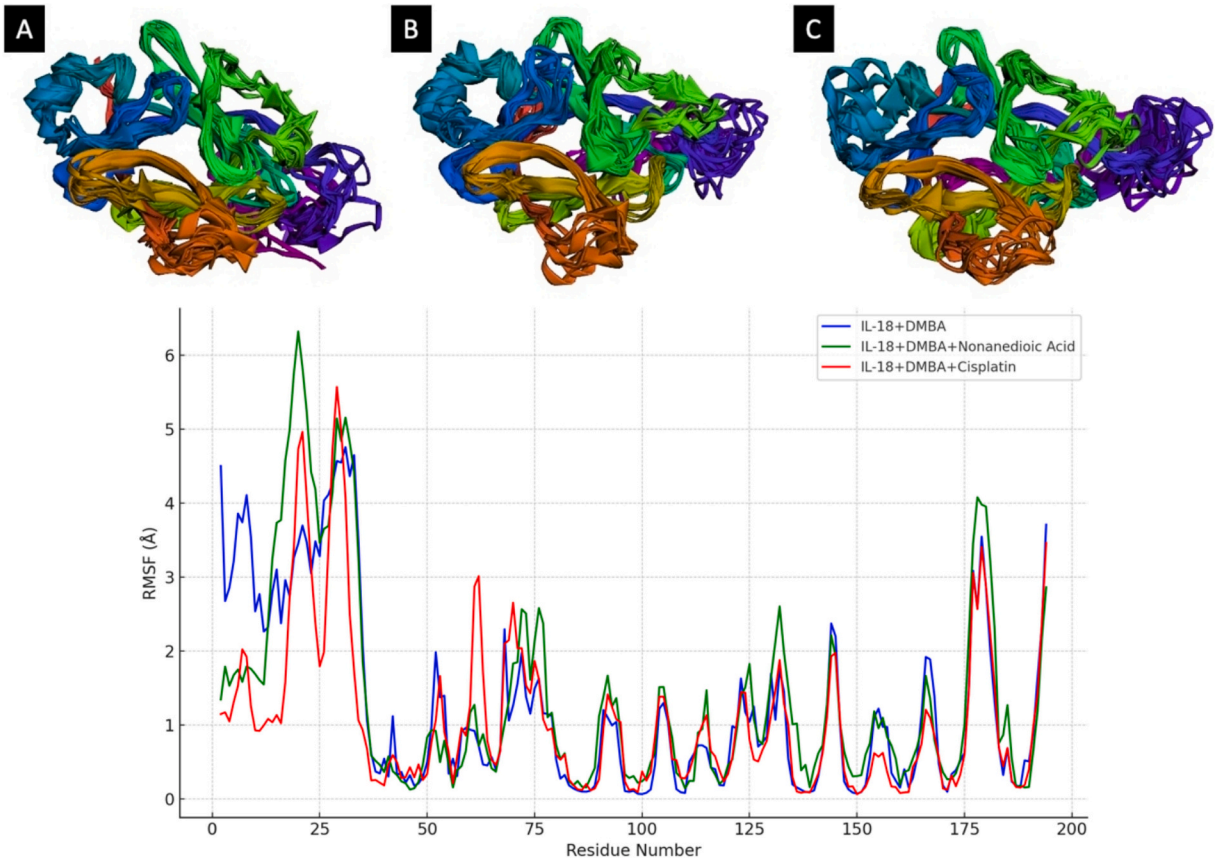

Fig. 12. 10 ns of IL-18 Complex, IL-18 + DMBA (A), (IL-18 + DMBA) + Cisplatin (B), (IL-18 + DMBA) + Nonanedioic acid (C).

values indicate the presence of anaemia or another underlying medical condition (Virdee et al., 2020). Erythrocytes possess multiple antioxidant systems that allow them to manage significant oxidative damage. In addition, elevated levels of SGOT and SGPT may indicate the presence of cancer, but this is not always the case (Li et al., 2023; Virdee et al., 2020). In the untreated cancer group (C-), the levels of IL-1β were significantly elevated. Multiple characteristics of immune cells, angiogenesis, migration, proliferation, and metastases are impacted by this cytokine. Furthermore, administering herbal remedies that are abundant in antioxidants and compounds that combat cancer might diminish the synthesis of IL-1β by cancerous or immune cells, so exerting an opposing influence on the progression of cancer (Ali et al., 2023). GB includes Quercetine, a compound that exhibits pro-inflammatory effects. In ARPE-19 cells, IL-1β significantly raises the levels of ICAM-1, sICAM-1, IL-6, IL-8, and MCP-1, both in terms of protein and gene expression. Quercetin significantly reduced the levels of cytokines and chemokines in IL-1β-stimulated ARPE-19 cells by inhibiting signaling pathways involved in inflammation. This prevention of MAPK, NF-κB p65, IKKα/β, c-Jun, CREB, and ATF2 phosphorylation and NF-κB p65 translocation into the nucleus were the means by which this suppression was accomplished (Cheng et al., 2019). *Gynura procumbens* contains apigenin and kaempferol, which can decrease the degree of inflammation by decreasing the release of the pro-inflammatory cytokine TNF-α. Additionally, resveratrol and kaempferol can enhance the production of the anti-inflammatory cytokine IL-10 (Kim et al., 2021; Palacz-Wrobel et al., 2017). Administration of this herbal supplement leads to a dose-dependent rise in the production of IL-6 and IL-10. Studies indicate that *Gynura procumbens* possesses notable advantages due to its abundance of anti-inflammatory compounds such as apigenin, quercetin, and kaempferol (Palacz-Wrobel et al., 2017).

Histopathological analysis demonstrated that treatment with GB extract markedly reinstated cervical tissue architecture. The epithelial lining was continuous and homogeneous, exhibiting diminished nuclear pleomorphism and reduced inflammatory infiltration relative to the DMBA-only group. Significantly, diminished indications of dysplasia and cellular atypia were noted. In comparison to cisplatin, GB therapy produced less severe histological changes. Cisplatin-treated tissues exhibited indications of cytotoxic stress, such as epithelial thinning and nuclear shrinkage, whereas the GB group displayed enhanced epithelial integrity and a more organised cellular structure. These data indicate that GB provides a protecting and maybe regenerating impact on cervical epithelium, unlike the more aggressive action of cisplatin ($p < 0.05$). The potential interaction between phytochemicals and conventional chemotherapeutic drugs is a vital aspect of translational research. This study did not directly investigate the co-administration of GB extract with cisplatin; however, emerging evidence indicates that phytochemicals possessing antioxidant and anti-inflammatory properties may synergistically enhance the efficacy of cisplatin by sensitizing tumor cells, promoting apoptosis, and mitigating chemotherapy-induced toxicity (Dasari et al., 2022). Compounds including flavonoids and polyunsaturated fatty acids, identified in the extract, have exhibited similar effects in other models. However, the antioxidant properties of these chemicals may diminish the efficiency of cisplatin by neutralizing reactive oxygen species integral to its mechanism of action (Jomova et al., 2023). Consequently, additional research is necessary to ascertain the therapeutic compatibility and best dose regimen for the combination of GB and cisplatin in cancer therapy. The process via which GB components access cervical tissue is probably facilitated by systemic absorption and dispersion. Numerous essential chemicals in the extract, including flavonoids and unsaturated fatty acids, exhibit lipophilicity and are easily absorbed in the gastrointestinal tract. After ingestion, they circulate through the bloodstream and may accumulate in inflamed or neoplastic tissues due to heightened vascular permeability and local biochemical signals. While direct tissue concentration

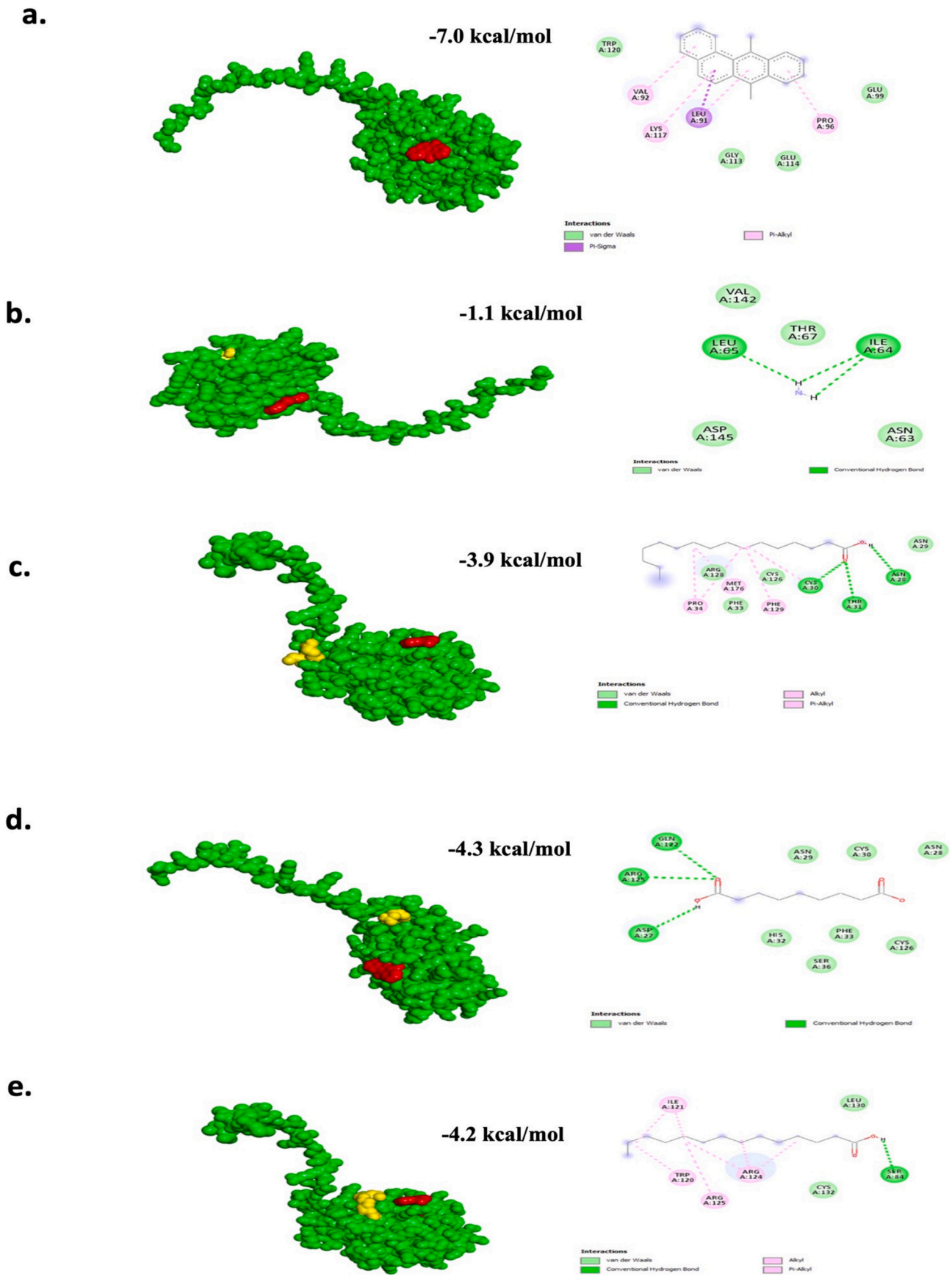

Fig. 13. IL-10 + DMBA (A), (IL-10 + DMBA) + Cisplatin (B), (IL-10 + DMBA) + n-Hexadecanoic (C), (IL-10 + DMBA) + Nonanedioic acid (D), (IL-10 + DMBA) + Tetradecanoic acid (E).

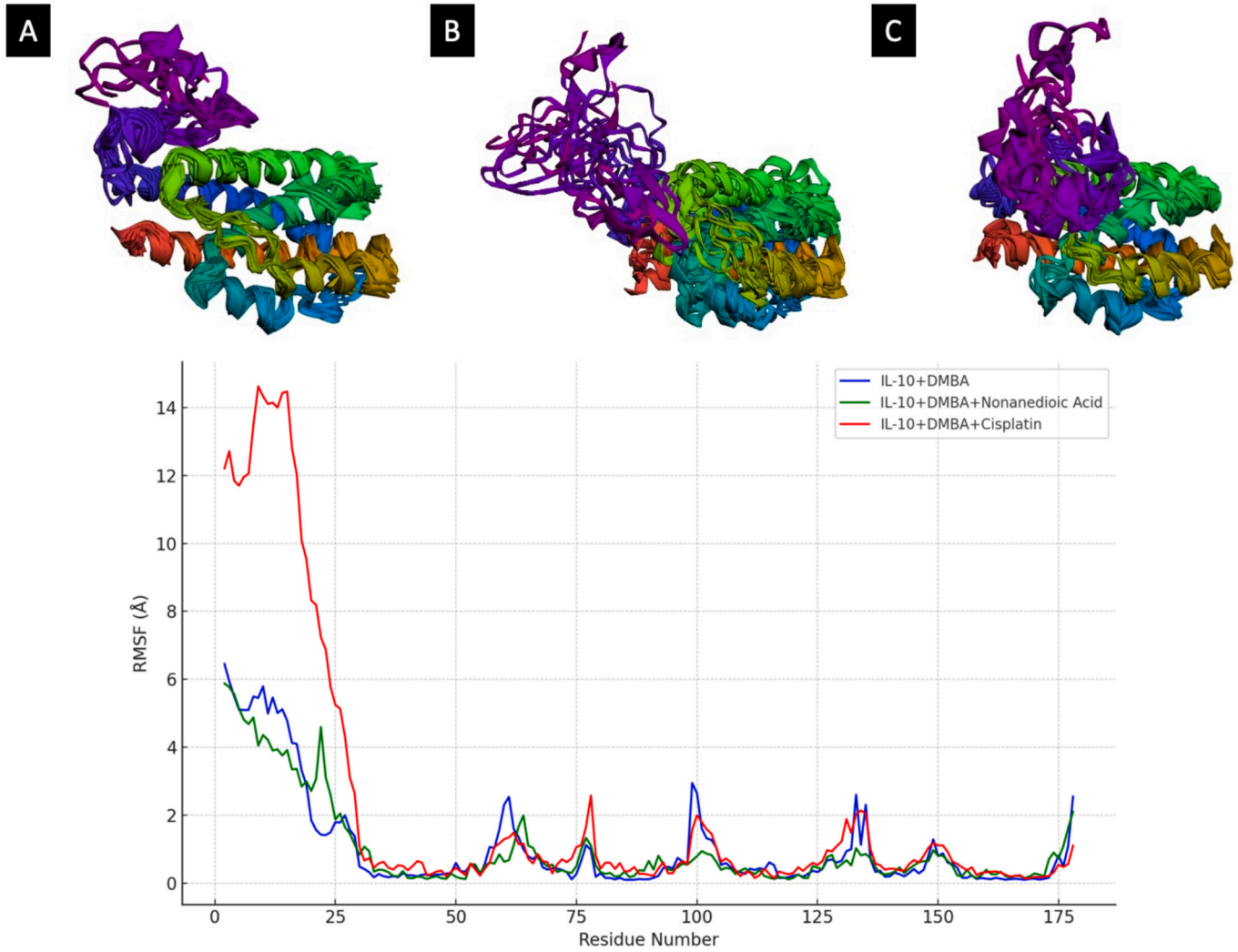

Fig. 14. 10 ns of IL-10 Complex, IL-10 + DMBA (A), (IL-10 + DMBA) + Cisplatin (B), (IL-10 + DMBA) + Nonanedioic acid (C).

was not quantified in this investigation, the noted histological and cytokine enhancements imply effective bioavailability at the target location (Losada-Barreiro et al., 2022). Subsequent pharmacokinetic investigations, encompassing tissue distribution analysis, are essential to validate these hypotheses.

The treatment of *Gynura procumbens* leaf extract enhances the proliferation of cervical cellular tissue. Microscopic changes were observed at dosages of 200 and 300 mg/kg body weight. The GB group, which received the lowest dosage, demonstrated the highest expression of IL-18, similar to the group of rat with a cervical cancer model. The researchers discovered that tumor patients exhibiting increased IL-18 protein levels may get advantages from antioxidants sourced from GB to diminish nuclear factor-κB activation (NF-κB), consequently lowering IL-18 production in tumors by suppressing NF-κB activity (Tan et al., 2020). The study indicated that reactive oxygen species (ROS) in cervical tumor tissue influenced the expression of interleukin-18 (IL-18) (Briukhovetska et al., 2021). Given that interleukins are proteins of significant immunological importance and substantially influence cancer biology, their study is crucial for understanding cancer therapeutic mechanisms (Briukhovetska et al., 2021). Interleukins can modulate tumor growth by either promoting or inhibiting it (Briukhovetska et al., 2021; Anestakis, 2015). The effects of various interleukins on the progression and metastasis of cancer can vary depending on the specific circumstances and type of cancer. Variations in IL-6 levels, especially within the GB3 group (rats treated with DMBA +300 mg/kg BW of GB), may be ascribed to the presence of n-Hexadecanoic acid and its detrimental interactions, including the donor-donor interaction with Threonine (THR A:167). Nonetheless, the prevailing trend suggests that the active compounds exhibit superior efficacy compared to cisplatin, hence confirming the therapeutic promise of Sambung Nyawa. This disparity may be attributed to the adverse acceptor-acceptor interaction involving Nonanedioic acid. Nonetheless, the overall data indicate that the active compounds exhibit superior performance compared to cisplatin, highlighting their therapeutic potential. Based on Moleculer Dynamic modeling, the attenuation of these significant fluctuations suggests that nonanedioic acid may facilitate more effective interactions with IL-18, thereby enhancing therapeutic uses by stabilizing critical areas of the protein structure (Wibowo et al., 2021). Nonanedioic acid offers superior stability across critical functional domains of the protein, perhaps leading to improved efficacy in medication formulations. The stability of these areas may assist in preserving the functional integrity of IL-10 under physiological circumstances.The persistent decrease in flexibility across several areas of IL-6 indicates that tetradecanoic acid serves as a more effective stabilizer, potentially minimizing structural alterations that could impact protein functionality in therapeutic applications. The observed reduction in flexibility may render tetradecanoic acid a viable candidate for improving the efficacy and stability of IL-6-targeted therapies. Subsequent study indicates that residues 100–130, which encompass critical structural elements, exhibit reduced flexibility in the cisplatin complex relative to n-hexadecanoic acid. Residue 120

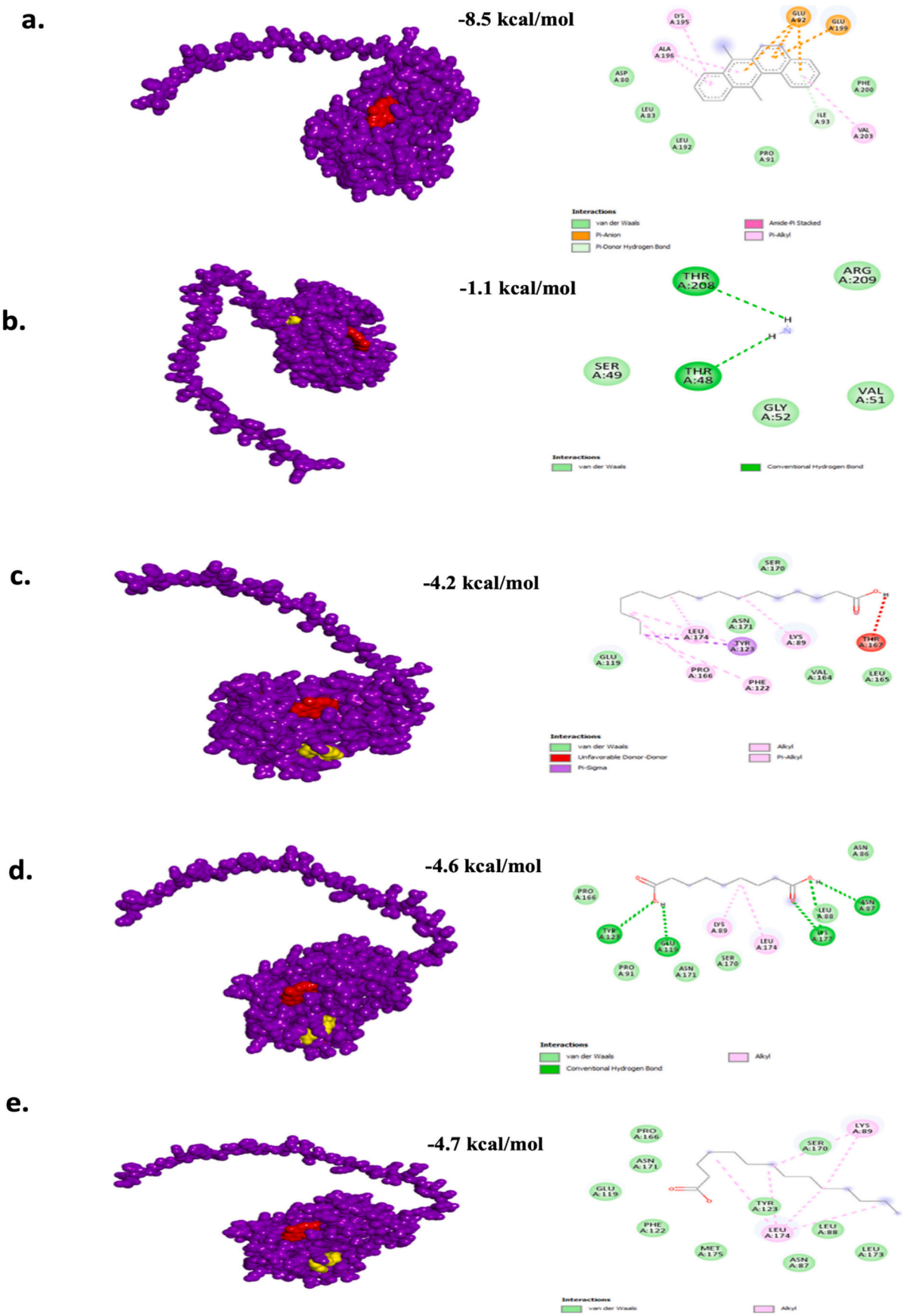

Fig. 15. IL-6 + DMBA (A), (IL-6 + DMBA) + Cisplatin (B), (IL-6 + DMBA) + n-Hexadecanoic (C), (IL-6 + DMBA) + Nonanedioic acid (D), (IL-6 + DMBA) + Tetradecanoic acid (E).

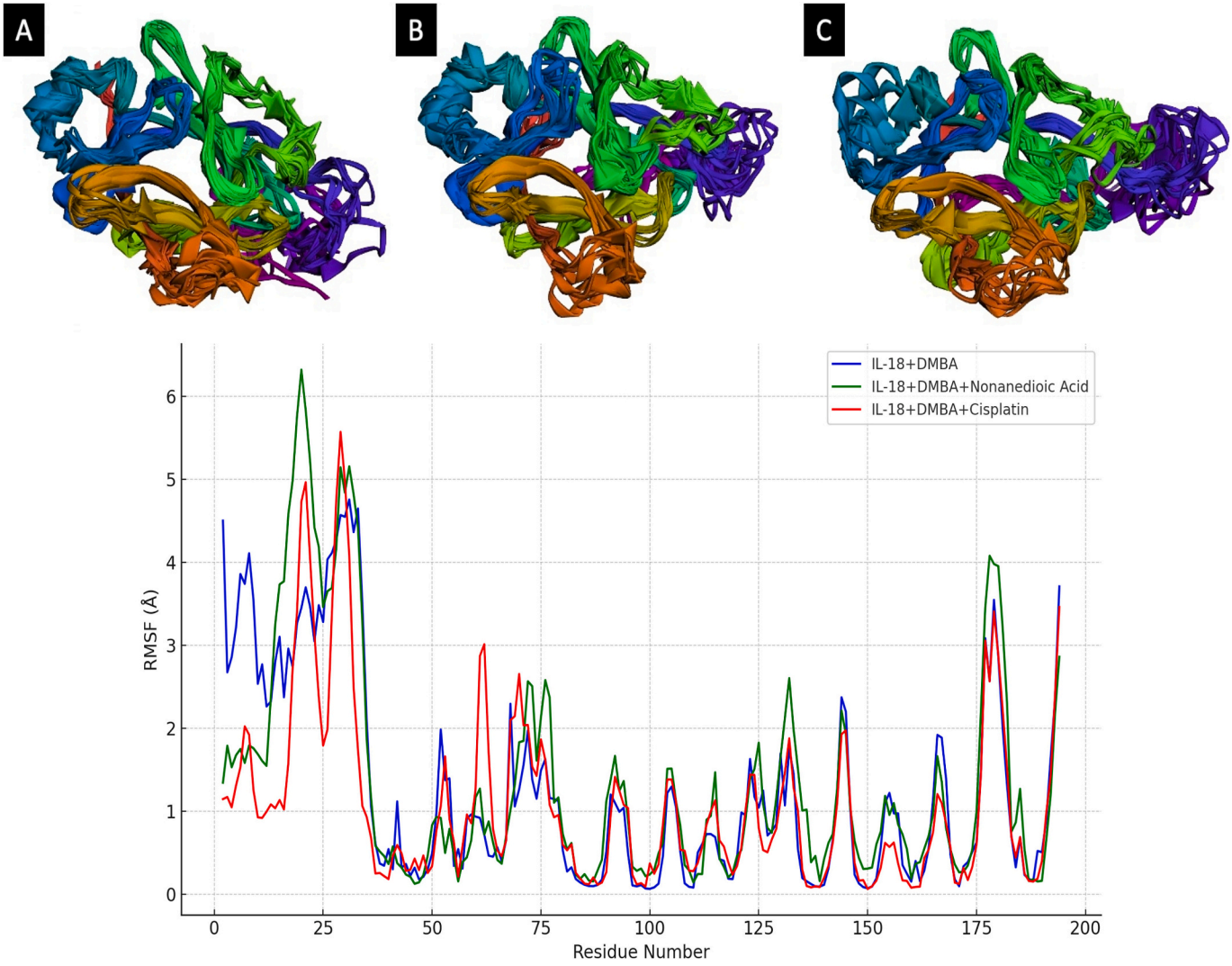

Fig. 16. 10 ns of IL-6 Complex, IL-6 + DMBA (A), (IL-6 + DMBA) + Cisplatin (B), (IL-6 + DMBA) + Nonanedioic acid (C).

exhibits an RMSF of 4.2 Å in the presence of cisplatin, however it demonstrates a greater value of 5.9 Å with n-hexadecanoic acid (Wibowo et al., 2022). This indicates that although n-hexadecanoic acid enhances overall flexibility, its impact is more significant in the N-terminal region, resulting in mild stabilization of other protein regions. The data indicates that n-hexadecanoic acid may have potential if the flexibility it produces can be optimized, particularly for targeted applications in certain protein areas (Wibowo et al., 2024).

The putative function of cytokinins in regulating oxidative stress in DMBA-induced cervical cancers merits consideration (Tomaziu-Todosia Anton et al., 2025). Cytokinins may facilitate the neutralization of reactive oxygen species (ROS) by augmenting the expression of natural antioxidant enzymes, including superoxide dismutase (SOD), catalase (CAT), and glutathione peroxidase (GPx). These enzymes promote the detoxification of superoxide anions and hydrogen peroxide, which are typically increased during DMBA-induced carcinogenesis (Tomaziu-Todosia Anton et al., 2025). Cytokinins additionally function via the Nrf2-ARE pathway to enhance antioxidant response components, and certain derivatives may have direct radical-scavenging activity. Cytokinins may reduce oxidative DNA damage and hence suppress tumor development by restoring cellular redox balance.This suggested mechanism enhances the observed histopathological changes and substantiates the therapeutic potential of GB in this model. Recent research underscores the role of particular signaling pathways in the cytokinin-induced decrease of ROS (Hammad et al., 2023). The activation of the Nrf2-ARE pathway is a crucial mechanism that governs the transcription of antioxidant defense genes such as SOD, CAT, and GPx. Cytokinins augment Nrf2 nuclear translocation and its binding to ARE sequences, hence increasing the endogenous antioxidant system during oxidative stress conditions induced by DMBA exposure. Cytokinins may also interact with redox-sensitive elements of the MAPK pathway, consequently affecting cellular stress responses and apoptosis. Cytokinins, via these signaling cascades, scavenge ROS and regulate stress-related gene expression, thereby safeguarding cervical tissues from oxidative damage (Ngo & Duennwald, 2022). Cytokinins demonstrate selective immunomodulatory actions via modulating inflammatory signaling pathways. The observed suppression of IL-1β and IL-18 in this study may be ascribed to the downregulation of inflammasome activity, specifically NLRP3, essential for the maturation of these cytokines (Hammad et al., 2023). Cytokinins may prevent the activation of caspase-1, hence further restricting the production of IL-1 family cytokines. The enhancement of IL-6 and IL-10 expression may be associated with cytokinin-induced activation of the STAT3 pathway, which is essential for resolving inflammation and facilitating tissue regeneration. Cytokinins also regulate essential transcriptional factors, including NF-κB and MAPKs (Cheng et al., 2019). Cytokinins diminish the production of pro-inflammatory mediators and augment anti-inflammatory responses by decreasing NF-κB nuclear translocation and attenuating the

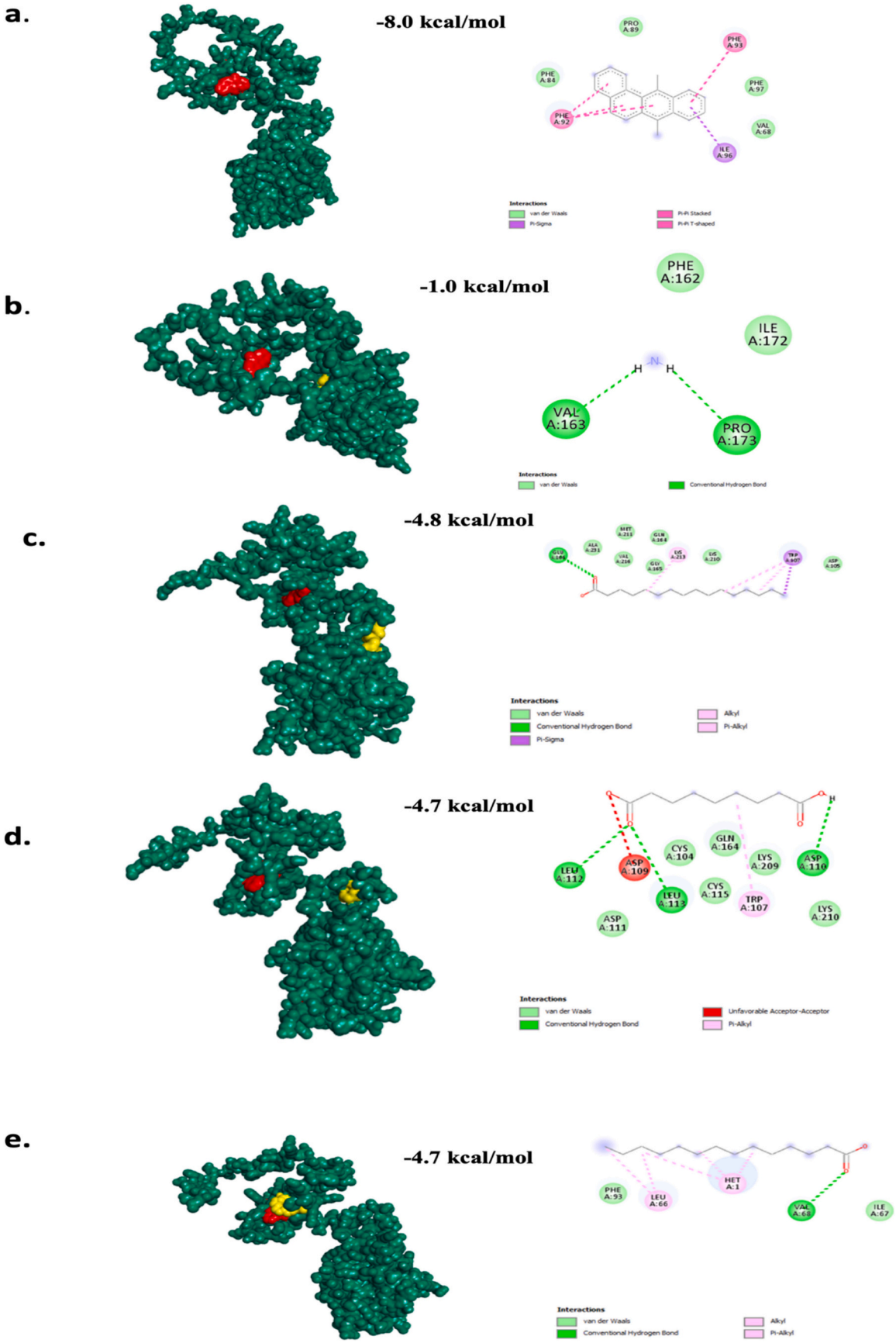

Fig. 17. IL-1β + DMBA (A), (IL-1β + DMBA) + Cisplatin (B), (IL-1β + DMBA) + n-Hexadecanoic (C), (IL-1β + DMBA) + Nonanedioic acid (D), (IL-1β + DMBA) + Tetradecanoic acid (E).

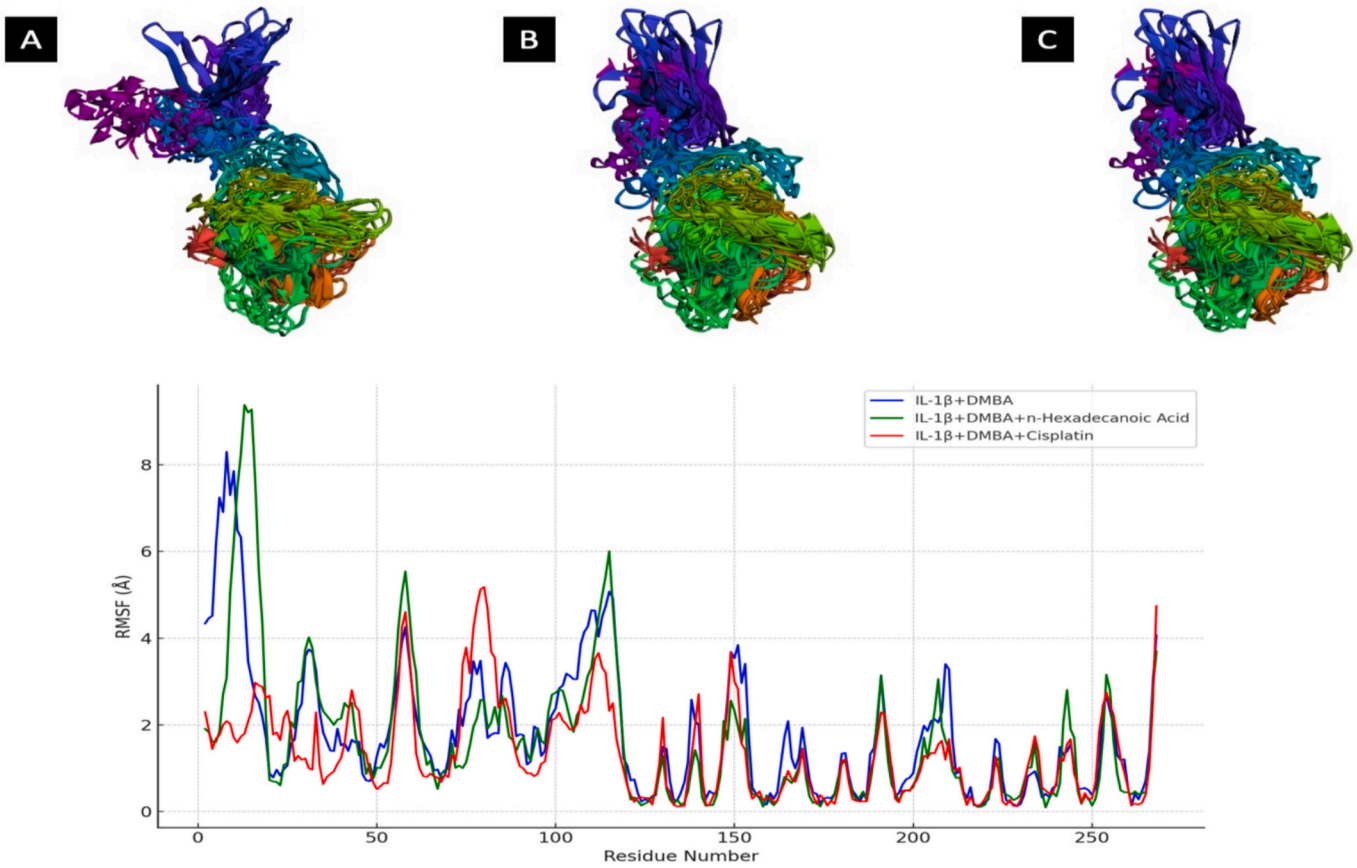

Fig. 18. 10 ns of IL-1β Complex, IL-1β + DMBA (A), (IL-1β + DMBA) + Cisplatin (B), (IL-1β + DMBA) + Nonanedioic acid (C).

phosphorylation of MAPK components (ERK, JNK, and p38) (Tomaziu-Todosia Anton et al., 2025; Cambon et al., 2025). These processes offer a thorough elucidation of the cytokine expression profile found in the DMBA-induced cervical carcinoma model.

5. Conclusion

The chemicals in this plant can reduce the production of IL-1β and IL-18 in cervical cells in blood and tissue, which in turn increases the expression of IL-6 and IL-10. The data indicate that nonanedioic acid and tetradecanoic acid demonstrate enhanced interactions on IL-18 expression in cisplatin, resulting in increased overall IL-10 expression in *Gynura procumbens* -treated animals. These active chemicals have enhanced therapeutic efficacy, especially in stabilizing the structures of critical proteins including IL-10 and IL-6. Comprehensive results, both in silico and in vivo, substantiate that these chemicals may present a more efficacious alternative to cisplatin in therapeutic applications. Future research should concentrate on enhancing the advantageous properties of these acids for specific protein interactions.

CRediT authorship contribution statement

Putri Cahaya Situmorang: Writing – review & editing, Writing – original draft, Supervision, Formal analysis, Data curation, Conceptualization. **Syahputra Wibowo:** Writing – review & editing, Writing – original draft, Visualization, Validation, Conceptualization. **Syafruddin Ilyas:** Writing – review & editing, Investigation, Funding acquisition, Formal analysis, Data curation. **Sony Eka Nugraha:** Writing – review & editing, Writing – original draft, Resources, Project administration, Methodology, Investigation, Funding acquisition, Formal analysis. **Alexander Patera Nugraha:** Writing – review & editing, Software, Resources, Project administration. **Diyah Tri Utami:** Writing – review & editing, Validation, Methodology, Investigation. **Nik Mohd Afizan Nik Abd Rahman:** Writing – review & editing, Supervision, Formal analysis. **Rizal Mukra:** Writing – review & editing, Software, Resources.

Funding statement

This research was support by the "LPDP in Equity project research PKUU-PT QS WUR RANK 102–300 scheme under contract numbers 7092.1/UN5.1.R/PPM/2023 and 8/UN5.2.3.1/PPM/KPEP/2023.

Declaration of competing interest

The authors declare the following financial interests/personal relationships which may be considered as potential competing interests: Putri Cahaya Situmorang reports article publishing charges was provided by Universitas Sumatera Utara. If there are other authors, they declare that they have no known competing financial interests or personal relationships that could have appeared to influence the work reported in this paper.

Appendix A. Supplementary data

Supplementary data to this article can be found online at https://doi.org/10.1016/j.jff.2025.106963.

Data availability

Data will be made available on request.

References

Abotaleb, M., Liskova, A., Kubatka, D., & Büsselberg, P. (2020). Therapeutic potential of plant phenolic acids in the treatment of Cancer. *Biomolecules, 10*(2), 221. https://doi.org/10.3390/biom10020221

Ali, M., Wani, S.U.D., Salahuddin, M., S N M,Dey,T., Zargar, M.I., Singh, J., 2023. Recent advance of herbal medicines in cancer- a molecular approach. Heliyon 9(2): e13684. doi: https://doi.org/10.1016/j.heliyon.2023.e13684.

Anisimov, V. N., Zabezhinski, M. A., Popovich, I. G., Zaripova, E. A., Musatov, S. A., Andre, V., … Sichel, F. (2000). Inhibitory effect of melatonin on 7, 12-dimethylbenz [a]anthracene-induced carcinogenesis of the uterine cervix and vagina in mice and mutagenesis in vitro. *Cancer Letters, 156*(2), 199–205.

Baird, W. M., & Olsson, K. (1996). Mechanisms of 7,12-dimethylbenz[a]anthracene (DMBA)-induced skin carcinogenesis. *Carcinogenesis, 17*(11), 2217–2225. https://doi.org/10.1093/carcin/17.11.2217

Bostanci, N., & Emingil, G. (2016). Interleukin-6 and its role in oral cancer. *Journal of Periodontology, 87*(3), 282–292. https://doi.org/10.1902/jop.2015.150416

Briukhovetska, B., Dörr, J., Endres, S., Libby, P., Dinarello, C. A., & Kobold, S. (2021). Interleukins in cancer: From biology to therapy. *Nature Reviews. Cancer, 21*(8), 481–499. https://doi.org/10.1038/s41568-021-00363-z

Cambon, A., Guervilly, C., Delteil, C., Potere, N., Bachelier, R., Tellier, E., … Kaplanski, G. (2025). Caspase-1 activation, IL-1/IL-6 signature and IFNγ-induced chemokines in lungs of COVID-19 patients. *Frontiers in Immunology, 15*, 1493306. https://doi.org/10.3389/fimmu.2024.1493306

Cheng, S., Huang, W. C. S., Pang, J. H. S., Wu, Y. H., & Cheng, C. Y. (2019). Quercetin inhibits the production of IL-1β-induced inflammatory cytokines and chemokines in ARPE-19 cells via the MAPK and NF-κB signaling pathways. *International Journal of Molecular Sciences, 20*(12), 2957. https://doi.org/10.3390/ijms20122957

Choi, Y., & Lee, S. (2020). The role of interleukin-10 in cancer: A review. *Cancer Research and Treatment, 52*(3), 709–722. https://doi.org/10.4143/crt.2020.0422

Conney, A. H., & Chang, R. L. (1991). Role of cytochrome P-450 in the activation of polycyclic aromatic hydrocarbons. *Cancer Research, 51*(2), 369–377. https://pubmed.ncbi.nlm.nih.gov/1671396/.

Dasari, S., Njiki, S., Mbemi, A., Yedjou, C. G., & Tchounwou, P. B. (2022). Pharmacological effects of cisplatin combination with natural products in cancer chemotherapy. *International Journal of Molecular Sciences, 23*(3), 1532. https://doi.org/10.3390/ijms23031532

Giri, P., Camarillo, I. G., & Sundararajan, R. (2023). Enhancement of reactive oxygen species production in triple negative breast cancer cells treated with electric pulses and resveratrol. *Explor Target Antitumor Ther, 4*(1), 42–56. https://doi.org/10.37349/etat.2023.00122

Gopalakrishnan, V., & Thompson, E. W. (2022). Interleukin-18 and its role in inflammation and cancer. *Frontiers in Immunology, 13*, Article 799074. https://doi.org/10.3389/fimmu.2022.799074

Hammad, M., Raftari, M., Cesário, R., Salma, R., Godoy, P., Emami, S. N., & Haghdoost, S. (2023). Roles of oxidative stress and Nrf2 signaling in pathogenic and non-pathogenic cells: A possible general mechanism of resistance to therapy. *Antioxidants (Basel)., 12*(7), 1371. https://doi.org/10.3390/antiox12071371

Hashemzaei, M., Delarami Far, A., Yari, A., Heravi, R. E., Tabrizian, K., Taghdisi, S. M., et al. (2017). Anticancer and apoptosis-inducing effects of quercetin in vitro and in vivo. *Oncology Reports, 38*(2), 819–828. https://doi.org/10.3892/or.2017.5766

Hew, C. S., Khoo, B. Y., & Gam, L. H. (2013). The anti-cancer property of proteins extracted from *Gynura procumbens* (Lour.) Merr. *PLoS One, 11*(8), Article e68524. https://doi.org/10.1371/journal.pone.0068524

Ilyas, S., Murdela, F., Hutahaean, S., & Situmorang, P. C. (2019). The effect of Haramounting leaf ethanol extract (*Rhodomyrtus tomentosa* (Aiton) Hassk.) on the number of leukocyte type and histology of mice Pulmo (*Mus Musculus* L.) exposed to electronic cigarette. *Open access Macedonian J med sci., 7*(11), 1750–1756. https://doi.org/10.3889/oamjms.2019.467

Imran, M., Salehi, B., Sharifi-Rad, J., Aslam Gondal, T., Saeed, F., Imran, A., et al. (2019). Kaempferol: A key emphasis to its anticancer potential. *Molecules, 24*(12), 2277. https://doi.org/10.3390/molecules24122277

Jomova, K., Raptova, R., Alomar, S. Y., Alwasel, S. H., Nepovimova, E., Kuca, K., & Valko, M. (2023). Reactive oxygen species, toxicity, oxidative stress, and antioxidants: Chronic diseases and aging. *Archives of Toxicology, 97*(10), 2499–2574. https://doi.org/10.1007/s00204-023-03562-9

Kim, H. H., Ha, S. E., Vetrivel, P., Bhosale, P. B., Kim, S., & M., Kim G.S.. (2021). Potential antioxidant and anti-inflammatory function of *Gynura procumbens* polyphenols ligand. *International Journal of Molecular Sciences, 22*(16), 8716. https://doi.org/10.3390/ijms22168716

Lee, S. E., & Lee, M. A. (2018). Interleukin-6 as a critical mediator of cancer progression and metastasis. *Journal of Clinical and Experimental Hepatology, 8*(4), 437–442. https://doi.org/10.1016/j.jceh.2018.06.008

Li, J., Liang, L., Feng, L., Cao, S., Cai, Y.S., .Li, X., Qian, Z., et al., 2023. The prognostic value of blood eosinophil level in AECOPD is influenced by corticosteroid treatment during hospitalization. Journal of Inflammation Research 2(16): 3233–3243. doi: https://doi.org/10.2147/JIR.S421605.

Li, W., & Zhang, L. (2015). Mechanisms of DMBA-induced skin cancer and the role of DNA adducts in carcinogenesis. *Journal of Cancer Research and Clinical Oncology, 141*(10), 1899–1911. https://doi.org/10.1007/s00432-015-1957-7

Losada-Barreiro, S., Sezgin-Bayindir, Z., Paiva-Martins, F., & Bravo-Díaz, C. (2022). Biochemistry of antioxidants: Mechanisms and pharmaceutical applications. *Biomedicines, 10*(12), 3051. https://doi.org/10.3390/biomedicines10123051

Ma, Z., Kim, Y. M., Howard, E. W., Feng, X., Kosanke, S. D., Yang, S., … Yang, X. (2018). DMBA promotes ErbB2-mediated carcinogenesis via ErbB2 and estrogen receptor pathway activation and genomic instability. *Oncology Reports, 40*(3), 1632–1640. https://doi.org/10.3892/or.2018.6545

Manurung, R. D., Ilyas, S., Hutahaean, S., Rosidah, R., & Situmorang, P. C. (2021). Diabetic wound healing in FGF expression by Nano herbal of *Rhodomyrtus tomentosa* L. and *Zanthoxylum acanthopodium* fruits. *Pakistan J biological sci., 24*(3), 401–408. https://doi.org/10.3923/pjbs.2021.401.408

Nebert, D. W., & Dalton, T. P. (2006). The role of cytochrome P450 enzymes in the metabolism of 7,12-dimethylbenz[a]anthracene and other carcinogens. *Toxicology and Applied Pharmacology, 213*(1), 110–121. https://doi.org/10.1016/j.taap.2006.03.010

Ngo, V., & Duennwald, M. L. (2022). Nrf2 and oxidative stress: A general overview of mechanisms and implications in human disease. *Antioxidants (Basel)., 11*(12), 2345. https://doi.org/10.3390/antiox11122345

Palacz-Wrobel, P., Borkowska, M., Paul-Samojedny, M., Kowalczyk, M., Fila-Danilow, A., Suchanek-Raif, R., & Kowalski, J. (2017). Effect of apigenin, kaempferol and resveratrol on the gene expression and protein secretion of tumor necrosis factor alpha (TNF-α) and interleukin-10 (IL-10) in RAW-264.7 macrophages. *Biomedicine & pharmacotherapy =Biomedecine & pharmacotherapie., 93*, 1205–1212. https://doi.org/10.1016/j.biopha.2017.07.054

Pandey, P., Khan, F., Qari, H., & Oves, M. (2021). Rutin (bioflavonoid) as cell signaling pathway modulator: Prospects in treatment and chemoprevention. *Pharmaceuticals (Basel), 14(11)*, 1069. https://doi.org/10.3390/ph14111069

Pereira, R. M., & Silva, J. R. (2020). Inflammation and cytokines in cancer. *Cytokine, 136*, Article 155278. https://doi.org/10.1016/j.cyto.2020.155278

Rahmani, A. H., Almatroudi, A., Allemailem, K. S., Alwanian, W. M., Alharbi, B. F., Alrumaihi, F., … Almatroodi, S. A. (2023). Myricetin: A significant emphasis on its anticancer potential via the modulation of inflammation and signal transduction pathways. *International Journal of Molecular Sciences, 24*(110), 9665. https://doi.org/10.3390/ijms24119665

Shankar, E., Goel, A., Gupta, K., & Gupta, S. (2017). Plant flavone apigenin: An emerging anticancer agent. *Current Pharmacology Reports, 3*(6), 423–446. https://doi.org/10.1007/s40495-017-0113-2

Simanullang, R. H., Situmorang, P. C., Herlina, M., Noradina, B., Silalahi, M., & S.S.. (2022). Histological changes of cervical tumours following *Zanthoxylum acanthopodium* DC treatment, and its impact on cytokine expression. *Saudi J biological sciences, 29*(4), 2706–2718. https://doi.org/10.1016/j.sjbs.2021.12.065

Simanullang, R. H., Situmorang, P. C., Herlina, M., Noradina, B., & Silalahi.. (2022). Expression by Andaliman (*Zanthoxylum acanthopodium)* on cervical Cancer histology. *Pakistan J biological sciences, 25*(1), 49–55. https://doi.org/10.3923/pjbs.2022.49.55

Situmorang, P. C., & Ilyas, S. (2018). Description of testis histology of *Mus Musculus* after giving Nano herbal *Rhodomyrtus Tomentosa* (Haramonting). *Asian J Pharmaceutical and Clinical Research, 11*(11), 460–463. https://doi.org/10.22159/ajpcr.2018.v11i11.29042

Situmorang, P. C., Ilyas, S., Syahputra, R. A., Nugraha, A. P., Putri, M. S. S., & Rumahorbo, C. G. P. (2024). *Rhodomyrtus tomentosa* (Aiton) Hassk. (haramonting) protects against allethrinexposed pulmo damage in rats: Mechanistic interleukins. *Frontiers in Pharmacology, 15*, 1343936. https://doi.org/10.3389/fphar.2024.1343936

Situmorang, P. C., Ilyas, S., Syahputra, R. A., Sari, R. M., Nugraha, A. P., & Ibrahim, A. (2024). *Rhodomyrtus tomentosa* as a new anticancer molecular strategy in breast histology via Her2, IL33, EGFR, and MUC1. *Frontiers in Pharmacology, 15*, 1345645. https://doi.org/10.3389/fphar.2024.1345645

Stenbäck, F., Curtis, G., & Jacobs, A. J. (1989). Viral agents in two-stage cervical carcinogenesis: An experimental study in mice. *Gynecologic Oncology, 32*(2), 218–223. https://doi.org/10.1016/s0090-8258(89)80036-8

Tan, H. L., Chan, K. G., Pusparajah, P., Lee, H., & Goh, B. H. (2016). *Gynura procumbens:* An overview of the biological activities. *Frontiers in Pharmacology, 15*(7), 52. https://doi.org/10.3389/fphar.2016.00052

Tan, J. N., Mohd Saffian, S., Buang, F., Jubri, Z., Jantan, I., Husain, K., & Mohd, F. N. (2020). Antioxidant and anti-inflammatory effects of genus *Gynura*: A systematic review. *Frontiers in Pharmacology, 27(11)::504624*. https://doi.org/10.3389/fphar.2020.504624

Vannini, N., & Sasso, A. (2009). DNA damage and the role of ROS in DMBA-induced carcinogenesis. *Environmental and Molecular Mutagenesis, 50*(2), 74–81. https://doi.org/10.1002/em.20407

Virdee, P. S., Marian, I. R., Mansouri, A., Elhussein, L., Kirtley, S., Holt, T., & Birks, J. (2020). The full blood count blood test for colorectal Cancer detection: A systematic review, Meta-analysis, and critical appraisal. *Cancers (Basel), 12*(9), 2348. https://doi.org/10.3390/cancers12092348

Wibowo, S., Costa, J., Baratto, M. C., Pogni, R., Widyarti, S., Sabarudin, A., … Sumitro, S. B. (2022). Quantification and improvement of the dynamics of human serum albumin and glycated human serum albumin with Astaxanthin/Astaxanthin-metal ion complexes: Physico-chemical and computational approaches. *International Journal of Molecular Sciences, 23*(9), 4771. https://doi.org/10.3390/ijms23094771

Wibowo, S., Wardhani, S. K., Hidayati, L., Wijayanti, N., Matsuo, K., Costa, J., … Nuringtyas, T. R. (2024). Investigation of α-glucosidase and α-amylase inhibition for antidiabetic potential of agarwood (aquilaria malaccensis) leaves extract. *Biocatalysis and Agricultural Biotechnology, 58*, Article 103152. https://doi.org/10.1016/j.bcab.2024.103152

Wibowo, S., Widyarti, S., Sabarudin, A., Soeatmadji, D. W., & Sumitro, S. B. (2021). DFT and molecular dynamics studies of astaxanthin-metal ions (cu2+ and zn2+) complex to prevent glycated human serum albumin from possible unfolding. *Heliyon, 7*(3). https://doi.org/10.1016/j.heliyon.2021.e06548